

Matching Matters!

Ayres Freitas,¹ David López-Val,² and Tilman Plehn³

¹*PITT-PACC, Department of Physics & Astronomy, University of Pittsburgh, USA*

²*Centre for Cosmology, Particle Physics & Phenomenology CP3, Université catholique de Louvain, Belgium*

³*Institut für Theoretische Physik, Universität Heidelberg, Germany*

(Dated: August 27, 2018)

Effective Lagrangians are a useful tool for a data-driven approach to physics beyond the Standard Model at the LHC. However, for the new physics scales accessible at the LHC, the effective operator expansion is only relatively slowly converging at best. For tree-level processes, it has been found that the agreement between the effective Lagrangian and a range of UV-complete models depends sensitively on the appropriate definition of the matching. We extend this analysis to the one-loop level, which is relevant for electroweak precision data and Higgs decay to photons. We show that near the scale of electroweak symmetry breaking the validity of the effective theory description can be systematically improved through an appropriate matching procedure. In particular, we find a significant increase in accuracy when including suitable terms suppressed by the Higgs vacuum expectation value in the matching.

CONTENTS

I. Introduction	2
A. Effective Lagrangian	2
B. v -improved matching	3
C. Broken-phase matching	4
II. Oblique electroweak precision parameters	5
A. Effective Lagrangian	5
B. Higgs singlet extension	6
C. Scalar top partners	10
III. Higgs decay to photons	15
A. Effective Lagrangian	16
B. Higgs doublet extension	17
C. Scalar top partners	18
IV. Summary	21
References	21

I. INTRODUCTION

After the end of the LHC Run I and with the start of Run II, the field of particle physics has clearly entered a data-driven era. While we should not entirely dismiss our theoretical or experimental motivations to search for specific models of physics beyond the Standard Model, the amount of available LHC data requires a more model-independent language to analyze and communicate experimental results. This has led the Higgs [1–3], electroweak [4, 5], top [6], and dark matter [7] communities to employ effective Lagrangians or related methods to communicate LHC results. Another good example is the recent hint for a 750 GeV resonance, where the limited available data at best allows for an effective theory analysis. Nevertheless, the theory community also illustrated the limits of the effective theory approach by immediately linking the LHC anomaly to any number of models.

This strategy implies that independent of the effective theory being the main theoretical description of a given physics sector, the effective Lagrangian can serve as a means of communication between experiment and theory. To this end it is not necessary to show that an effective theory at the LHC is a fully consistent theory framework; instead, a given effective Lagrangian has to describe the effects of classes of new physics models at the LHC within the expected experimental precision. For Higgs signatures with a wide range of kinematic configurations this question has been studied at length, both for strongly and weakly interacting models [8–13]. It turns out that the expected measurement uncertainties largely limit us to tree-level effects of new physics, and that an appropriately defined dimension-6 Lagrangian description only breaks down in the presence of new resonance features.

In this paper we extend our effective Lagrangian considerations to systematically include quantum effects. We start by introducing two ways of improving the matching of the effective Lagrangian in Sec. IB and Sec. IC. Both of them target the problem that in the relevant region of parameter space the effective Lagrangian does not have a large scale hierarchy and instead we have to work under the weak condition that after electroweak symmetry breaking the new particles lie just above the weak scale, $v \lesssim \Lambda$.

We then study heavy particle loops contributing to electroweak precision observables (EWPO) in Sec. II. Two representative models for extended scalar sectors allow us to study the underlying features: an additional scalar electroweak singlet, and color-triplet heavy-quark scalar partners. We compute the oblique electroweak precision observables S and T in the full, UV-complete model as well as based on the effective Lagrangian. For the latter we explore several prescriptions for the one-loop matching. With the Higgs portal, contributions from loop-induced operators combine with loop insertions of tree-level operators. For the top partners all new physics effects appear through virtual heavy scalars and loop-induced operators. In addition, top partners feature in general two heavy scales, allowing us to test a dimension-6 description in the presence of multiple mass scales. All these are challenges which our matching prescription for the effective Lagrangian has to face.

Secondly, we study the loop-induced Higgs coupling to photons in Sec. III. Because a singlet Higgs portal hardly shows any features in this observable, we now test a two-Higgs doublet model including a charged Higgs boson, as well as the scalar top partner model mentioned above. Again, we show how the choice of matching procedure can significantly and systematically improve the agreement between the effective Lagrangian and the full models.

A. Effective Lagrangian

Effective field theories provide a useful language to communicate experimental results without having to specify any details of an underlying model. At energies below the characteristic UV scale of the new physics sector, only the light states are the physically accessible degrees of freedom. Based on the dynamic degrees of freedom at low energies, symbolically denoted as ϕ , and the underlying symmetries we define a Lagrangian of the kind

$$\mathcal{L}_{\text{eff}} = \mathcal{L}_{\text{SM}} + \sum_{d=5}^{\infty} \sum_{a_d} \frac{c_{a_d}^{(d)}}{\Lambda^{d-4}} \mathcal{O}_{a_d}^{(d)}, \quad (1)$$

where the heavy field dynamics is described by the Wilson coefficients $c_i(\mu)$. The effective operators $\mathcal{O}_i(\mu)$ parametrize the local interactions among the light states. The effective Lagrangian of Eq.(1) follows from averaging over short distance effects, which in the functional formalism of QFT means integrating out of the heavy field fluctuations in the UV action path integral [14, 15].

To relate the Wilson coefficients $c_i(\mu)$ to a set of full model parameters $g_j(\mu)$ we use the fact that, by construction, the effective Lagrangian reproduces the full model predictions in the low-energy range $E < \Lambda$. In quantum field theory observables are derived from one-particle-irreducible (1PI) n -point Greens functions. Therefore, we compute a set of renormalized 1PI Greens functions in the full model and based on the effective Lagrangian setups with help of the

packages FEYNARTS and FORMCALC [19]. Both of them we evaluate at an appropriate matching scale $\mu = \Lambda$,

$$\Gamma_{\text{full}}^{\text{1PI}}[\phi](g_j, \mu = \Lambda) = \Gamma_{\text{EFT}}^{\text{1PI}}[\phi](c_i, \mu = \Lambda). \quad (2)$$

The matching scale Λ is usually identified with the characteristic UV scale of the effective Lagrangian, above which the high-energy degrees of freedom start to be resolved.* Equation (2) allows us to express each Wilson coefficient in terms of the model parameters. For weakly coupled theories, the matching condition is applied order-by-order in the perturbative expansion, identifying the tree-level 1PI graphs first, and then moving to one-loop and beyond.

In this paper we assume a linear realization of electroweak symmetry breaking with a vacuum expectation value (vev) $v = 246$ GeV. We truncate our set of operators at dimension-6, which has been shown to be sufficient to describe (most of) the expected LHC observables. Some popular bases of these dimension-6 operators are the Warsaw [16], HISZ [5], and SILH bases [2]. All three maximize the use of bosonic operators to describe Higgs and electroweak observables. They can be mapped onto each other using equations of motion, integration by parts, field redefinitions, and Fierz transformations [17]. We use the SILH basis and retain only those operators relevant for Higgs physics at the LHC [2]. The effective Lagrangian truncated to dimension 6 reads

$$\begin{aligned} \mathcal{L}_{\text{EFT}} = \mathcal{L}_{\text{SM}} &+ \frac{c_H}{2\Lambda^2} \partial^\mu(\phi^\dagger \phi) \partial_\mu(\phi^\dagger \phi) + \frac{c_T}{2\Lambda^2} (\phi^\dagger \overleftrightarrow{D}^\mu \phi) (\phi^\dagger \overleftrightarrow{D}_\mu \phi) - \frac{c_6 \lambda}{\Lambda^2} (\phi^\dagger \phi)^3 \\ &+ \frac{ig c_W}{2\Lambda^2} (\phi^\dagger \sigma^k \overleftrightarrow{D}^\mu \phi) D^\nu W^k_{\mu\nu} + \frac{ig' c_B}{2\Lambda^2} (\phi^\dagger \overleftrightarrow{D}^\mu \phi) \partial^\nu B_{\mu\nu} \\ &+ \frac{ig c_{HW}}{\Lambda^2} (D^\mu \phi^\dagger) \sigma^k (D^\nu \phi) W^k_{\mu\nu} + \frac{ig' c_{HB}}{\Lambda^2} (D^\mu \phi^\dagger) (D^\nu \phi) B_{\mu\nu} \\ &+ \frac{g'^2 c_\gamma}{\Lambda^2} (\phi^\dagger \phi) B_{\mu\nu} B^{\mu\nu} + \frac{g_s^2 c_g}{\Lambda^2} (\phi^\dagger \phi) G^A_{\mu\nu} G^{\mu\nu A} \\ &- \left[\frac{c_u}{\Lambda^2} y_u (\phi^\dagger \phi) (\phi^\dagger \cdot \overline{Q}_L) u_R + \frac{c_d}{\Lambda^2} y_d (\phi^\dagger \phi) (\phi \overline{Q}_L) d_R + \frac{c_\ell}{\Lambda^2} y_\ell (\phi^\dagger \phi) (\phi \overline{L}_L) \ell_R + \text{h.c.} \right]. \quad (3) \end{aligned}$$

Here, $g = e/s_w, g' = e/c_w$, and g_s stand for the SM gauge couplings and λ denotes the usual Higgs quartic. The dimension-6 Wilson coefficients c_i are defined with a universal suppression of $1/\Lambda^2$ rather than the ad-hoc prior of $1/v^2$ or $1/m_W^2$ in the original proposal. The notation of the individual operators follows the notation for the Wilson coefficients, for example $\mathcal{O}_T \sim (\phi^\dagger \overleftrightarrow{D}^\mu \phi) (\phi^\dagger \overleftrightarrow{D}_\mu \phi)$.

B. v -improved matching

Whenever we discuss the validity of effective Lagrangian approaches we need to keep in mind that the matching of the individual Wilson coefficients to a given full model is not defined uniquely. This is particularly true when the matching scale is not far from the scale at which the electroweak symmetry is broken. A hierarchy of scales $\Lambda \gg v$ certainly justifies that we define an effective action by integrating out all heavy states in the unbroken phase $\langle \phi \rangle = 0$ and truncate that action only including terms up to the order $1/\Lambda^2$. The Wilson coefficients are by construction independent on the light field masses and low-scale parameters. In this ideal world of new physics governed by a single, very large energy scale, the default matching is free from ambiguities and leads to a rapidly converging effective field theory.

However, at hadron colliders, the numerator compensating the inverse powers of Λ can be any parameter with the appropriate mass dimension, including the partonic collider energy or masses induced by electroweak symmetry breaking. In addition, the relevant heavy mass scale does not have to be a Lagrangian parameter in some interaction basis, it can also be particle masses induced by other mechanism than electroweak symmetry breaking. Examples are vector fermion masses or supersymmetric partner masses, which receive dominant contributions from some heavy Lagrangian parameter, but subdominant effects from the electroweak vev. In this case, electroweak symmetry breaking will in general induce additional scales $\Lambda \pm gv$ from the new physics couplings to the Higgs. The default operator expansion in the unbroken phases removes all contributions of the type v/Λ from the definition of the matching scale and from the dimension-6 Wilson coefficients. If these corrections should be non-negligible it will fail to capture

* For LHC processes this statement is signature-dependent, because particles appearing, say, in the s -channel are much easier to resolve than particles in the t -channel. Similarly, particles appearing in loops are much harder to resolve than particles appearing at tree level. Clearly, any statement considering the quantitative validity of an effective Lagrangian needs to take these differences into account [11].

features of the full model. In that case, we can adapt the details of the matching scheme to enhance the level of agreement between the effective Lagrangian and the full model [11].

In our tree level analysis, we account for v -induced effects in two ways [11]: first, the matching scale Λ is not identified with a Lagrangian mass parameter in the unbroken phase, but with the mass of a physical particle. The masses of the heavy states can lead to more than one heavy scale, with the splitting generated by the electroweak vev. In this case, Λ is identified with the lightest new state by default.

Second, we allow for corrections suppressed by v/Λ in the Wilson coefficients. On the full model side we express the relevant observables in terms of model parameters in the mass-eigenstate Lagrangian, *i.e.* in terms of masses and mixing angles of the physical states. In this way, one effectively includes corrections from some higher-dimensional operators of the form $\mathcal{O}^{d=6+n} \sim \mathcal{O}^{d=6} \times (\phi^\dagger \phi)^n$, where the Higgs doublets appear as v -insertions in the broken phase.

We use the name v -improvement for the combination of these two steps. It is worth emphasizing that the v -improved prescription does not introduce additional free parameters, nor does it break any symmetries of the original Lagrangian. In that sense, it describes an equivalent effective Lagrangian. The v -improved matching of a linear realization of electroweak symmetry breaking is also different from the non-linear realization, because we still require that the Higgs boson forms a weakly coupled doublet with the Goldstone bosons.

C. Broken-phase matching

While the v -improvement described above is sufficient to systematically improve the agreement between the full model and the dimension-6 approximation, additional complications arise for loop-induced processes. As mentioned above, the functional approach to the effective Lagrangian is straightforward if the heavy sector can be fully separated from the light fields and integrated out in the path integral. In the case of mass eigenstates affected by mixing of heavy and a light field components, diagrammatic methods can improve the matching between the full theory and the effective Lagrangian [18]. As described in Sec. IA we use standard perturbation theory to compute a set of renormalized 1PI Greens functions to determine the Wilson coefficients order by order in the electroweak gauge coupling and in the mass dimension.

For the case of EW precision observables we rely on the renormalized one-loop gauge boson vacuum polarizations in the UV complete model,

$$\Pi_{VV}^{(R)}(p^2) = \Pi_{VV}(p^2) - (p^2 - m_V^2) \delta Z_V + \delta m_V^2. \quad (4)$$

The contributions to the un-renormalized Π_{VV} may be a combination of light, heavy, and mixed light-heavy field loops. All UV divergences are absorbed by the mass and wave function counter terms $\delta m_V^2, \delta Z_V$. In this expression we take the limit of large heavy masses and expand $\Pi_{VV}^{(R)}(p^2)$ in powers of v/Λ .

In complete analogy, we compute Π_{VV} as a function of the Wilson coefficients in the effective Lagrangian. Also here we can have two types of contributions: light particle loops including effective couplings induced at tree level, and tree-level insertions of loop induced operators. While the former are in general UV divergent, the latter include the relevant counter terms of the Wilson coefficients. Finally, we identify the two renormalized expressions for the Greens function and determine the finite parts of the renormalized Wilson coefficients. We will illustrate for our different examples how this matching procedure based on Greens functions leads to additional contributions to the Wilson coefficients compared to the functional approach.

From the field theory point of view, it is interesting to compare this approach to a leading-log resummation: the scale dependence $c_i(\mu)$ is the key element which relates the high-scale and low-scale regimes in the effective Lagrangian. We always start with the effective Lagrangian in the unbroken high-scale phase and for instance integrate out the gauge invariant and separately renormalizable heavy sector/heavy fields. Then we match the effective Lagrangian to the full model at the intrinsic heavy mass scale $\Lambda = \sqrt{2\lambda_2} v_s^2$. To get to the physically relevant energy scales we can either evolve the running Wilson coefficients to the low scale below electroweak symmetry breaking; or we introduce explicit counterterms for the Wilson coefficients entering the low-scale Greens functions, mixing the different dimension-6 operators. Both ways consistently extend the effective Lagrangian to the broken phase and have to lead to the same predictions — to leading-log accuracy in the first case and exactly to fixed order in the second.

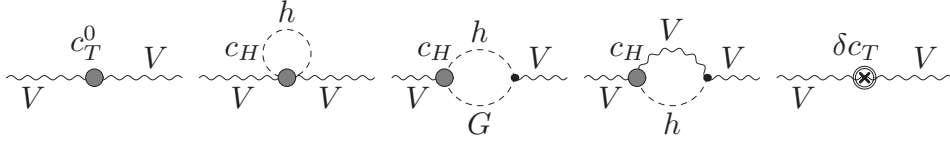


Figure 1. Generic Feynman diagrams for the weak boson self-energies using a dimension-6 effective Lagrangian [19]. The shaded dots denote the dimension-6 operators.

II. OBLIQUE ELECTROWEAK PRECISION PARAMETERS

Effects of new physics on the electroweak gauge sectors can be approximately described in terms of oblique parameters. The two most relevant parameters constraining large classes of models are

$$\begin{aligned} \frac{\alpha_{\text{em}}}{4s_w^2 c_w^2} S &= \left[-\Pi'_{\gamma\gamma} + \Pi'_{ZZ} - \Pi'_{\gamma Z} \frac{c_w^2 - s_w^2}{c_w s_w} \right] - [\dots]_{\text{SM}} \\ \alpha_{\text{em}} T &= [\Pi_{WW} - \Pi_{ZZ}] - [\dots]_{\text{SM}} . \end{aligned} \quad (5)$$

The self energies $\Pi^{(\prime)}$ are evaluated at zero momentum transfer and can be defined by the dimension-4 Lagrangian

$$\begin{aligned} \mathcal{L} = \mathcal{L}_{\text{SM}} &- \frac{\Pi'_{\gamma\gamma}}{4} F_{\mu\nu} F^{\mu\nu} - \frac{\Pi'_{WW}}{2} W_{\mu\nu} W^{\mu\nu} - \frac{\Pi'_{ZZ}}{4} Z_{\mu\nu} Z^{\mu\nu} - \frac{\Pi'_{\gamma Z}}{4} F_{\mu\nu} Z^{\mu\nu} \\ &- \Pi_{WW} m_W^2 W_\mu^+ W^{-\mu} - \frac{\Pi_{ZZ}}{2} m_Z^2 Z_\mu Z^\mu , \end{aligned} \quad (6)$$

using the standard definitions of the field strengths after electroweak symmetry breaking. Some contributions to $\Pi^{(\prime)}$ are already induced through Standard Model loops, which are removed through the above definition of the parameters S and T .

The self energy diagrams are by definition evaluated at zero momentum transfer, which means that the only scales which enter are the weak gauge boson and Higgs boson masses and, in case of new physics contributions, the masses of the new particles.

A. Effective Lagrangian

The definition of the oblique parameters Eq.(6) and some terms in the effective Lagrangian of Eq.(3) are similar in structure. Comparing them we see that new physics effects in the dimension-6 Lagrangian contribute to the $\Pi^{(\prime)}$ in two ways: First, loop-induced dimension-6 operators directly contribute to S and T at tree level. Some corresponding Feynman diagrams are shown in Fig. 1. The corresponding Wilson coefficients are of the order α_{em} , and we have to include the appropriate counter terms to renormalize the Wilson coefficients. In the operator basis of Eq.(3) the Wilson coefficient c_T is responsible for T , while a combination of c_B and c_W generates a non-zero S parameter,

$$\alpha_{\text{em}} T \Big|_{\text{tree insertion}} = c_T \frac{v^2}{\Lambda^2} , \quad S \Big|_{\text{tree insertion}} = 4\pi \frac{v^2}{\Lambda^2} (c_W + c_B) . \quad (7)$$

Second, we can insert operators generated at tree level into Standard Model one-loop diagrams, as shown in Fig. 1. These operators obviously only exist for models where there are relevant electroweak Wilson coefficients induced at tree level. In that case their contributions to S and T are also of order $\alpha_{\text{em}}/\Lambda^2$. To illustrate their structure we look at a generic tree-level-induced Wilson coefficient c_H . The two relevant self energy contributions for T in the limit of zero momentum transfer have similar structures,

$$\begin{aligned} \Pi_{WW} &= \frac{\alpha_{\text{em}} c_H v^2}{16\pi s_w^2 \Lambda^2} \left[3\Delta_\epsilon - 4 \log \frac{m_h^2}{\mu^2} + \frac{5}{2} - \frac{m_h^2}{2m_W^2} + \log \frac{m_W^2}{\mu^2} - \frac{4m_W^2 - m_h^2}{m_h^2 - m_W^2} \log \frac{m_h^2}{m_W^2} \right] \\ \Pi_{ZZ} &= \frac{\alpha_{\text{em}} c_H v^2}{16\pi s_w^2 c_w^2 \Lambda^2} \left[3\Delta_\epsilon - 4 \log \frac{m_h^2}{\mu^2} + \frac{5}{2} - \frac{m_h^2}{2m_Z^2} + \log \frac{m_Z^2}{\mu^2} - \frac{4m_Z^2 - m_h^2}{m_h^2 - m_Z^2} \log \frac{m_h^2}{m_Z^2} \right] , \end{aligned} \quad (8)$$

with $\Delta_\epsilon \approx 2/(4-n)$ describing the ultraviolet divergence. This divergence needs to be absorbed by renormalizing the Wilson coefficients c_T in the tree-level relation in Eq.(7). The counter term of c_T or, alternatively, its anomalous dimension can be linked to c_T - c_H operator mixing at one loop and is of the form $\delta c_T \propto \alpha_{\text{em}} c_H$. Altogether, the ultraviolet poles cancel and all contributions combine to a finite contribution

$$\alpha_{\text{em}} T \Big|_{\text{weak loops}} = \frac{3\alpha_{\text{em}} c_H v^2}{16\pi s_w^2 m_W^2 \Lambda^2} \left[\frac{m_Z^2 m_h^2}{m_h^2 - m_Z^2} \log \frac{m_h^2}{m_Z^2} - \frac{m_W^2 m_h^2}{m_h^2 - m_W^2} \log \frac{m_h^2}{m_W^2} \right], \quad (9)$$

which breaks custodial symmetry. The explicit logarithms induced by the weak-scale loops are of the kind $\log(m_h/m_V)$ with $V = W, Z$, and $m_h = 126$ GeV denoting the Standard Model Higgs mass. They are indicative of the aforementioned violation of custodial symmetry: while at tree level c_H does not violate custodial symmetry, at loop level it can mix with the other Wilson coefficients like c_T through its anomalous dimension. The resulting contribution to the T parameter will then be proportional to the logarithm of the scale splitting.

As discussed in Sec. I C, at this order in perturbation theory we need to include both, weak-scale loops combined with tree-level operators and tree-level diagrams with loop-induced operators. They arise at the same level of perturbation theory from the same dimension-6 Lagrangian. In contrast, a finite contribution to U only occurs once we include operators of higher mass dimension. The renormalization scale of Wilson coefficients is naturally chosen to be of the order of the electroweak scale, $\mu \sim m_W \sim m_Z \sim m_h \sim v$. In our numerical evaluation we fix $\mu = m_W$. For high-scale matching, the renormalization scale dependence defines a leading-log approximation of the Wilson coefficients in terms of $\alpha_{\text{em}} \log(\Lambda/m_W)$ [20]. This implies that dimension-6 contributions to both oblique parameters have leading contributions of the kind

$$\alpha_{\text{em}} T \sim c_j(\mu = m_W) \frac{\alpha_{\text{em}} v^2}{\Lambda^2} \log \frac{\Lambda^2}{m_W^2} \sim \alpha_{\text{em}} S, \quad (10)$$

as well as sub-leading contributions without this, often not very large, logarithm.

B. Higgs singlet extension

A Higgs singlet extension or (renormalizable) Higgs portal is defined by the extended scalar potential

$$V(\phi, S) = \mu_1^2 (\phi^\dagger \phi) + \lambda_1 |\phi^\dagger \phi|^2 + \mu_2^2 S^2 + \lambda_2 S^4 + \lambda_3 |\phi^\dagger \phi| S^2. \quad (11)$$

It contributes to the oblique parameters in both ways described in Sec. II A because of the linear coupling of the heavy scalar to the light Higgs doublet, $\mathcal{L} \supset \lambda_3 v_s S \phi^\dagger \phi$, with $\langle S \rangle = v_s/\sqrt{2}$ [21]. The interplay between the tree-level insertion of loop-induced operators and the loop-insertion of tree-level-induced operators is the reason why this model is interesting to study. The Higgs portal coupling λ_3 induces a finite mixing angle α [11]

$$\frac{\tan^2(2\alpha)}{4} = \frac{1}{4} \left(\frac{\lambda_3 v v_s}{\lambda_2 v_s^2 - \lambda_1 v^2} \right)^2 \stackrel{v \ll v_s}{\approx} \frac{\lambda_3^2 v^2}{4\lambda_2^2 v_s^2} \approx \frac{\lambda_3^2 v^2}{2\lambda_2 m_H^2} \approx s_\alpha^2 \quad \text{with} \quad m_H^2 \approx 2\lambda_2 v_s^2, \quad (12)$$

from the interaction eigenstates to the two mass eigenstates h and H . All approximations indicated by ‘ \approx ’ are leading in terms of v^2/Λ^2 . Explicit contributions from the new scalar are proportional to $s_\alpha^2 \equiv \sin^2 \alpha$, while the modified contribution from the Standard Model Higgs come with $c_\alpha^2 - 1 = -s_\alpha^2$. This means that the oblique parameters have the particularly simple leading behavior [10, 15]

$$\begin{aligned} S &\approx \frac{s_\alpha^2}{12\pi} \left(-\log \frac{m_h^2}{m_Z^2} + \log \frac{m_H^2}{m_Z^2} \right) \approx \frac{\lambda_3^2}{24\pi\lambda_2} \frac{v^2}{m_H^2} \log \frac{m_H^2}{m_h^2} \\ T &= \frac{-3s_\alpha^2}{16\pi s_w^2 m_W^2} \left(m_Z^2 \log \frac{m_H^2}{m_h^2} - m_W^2 \log \frac{m_H^2}{m_h^2} \right) \approx \frac{-3\lambda_3^2 v^2}{32\pi s_w^2 \lambda_2 m_W^2} \left(\frac{m_Z^2}{m_H^2} - \frac{m_W^2}{m_H^2} \right) \log \frac{m_H^2}{m_h^2}. \end{aligned} \quad (13)$$

While decoupling is guaranteed by the suppressed mixing angle $s_\alpha \propto 1/m_H$, we notice the additional logarithms $\log(m_H/m_h)$, which delay the decoupling of the heavy scalar. In the absence of a large hierarchy of scales we will see that the matching of the full theory to the truncated Lagrangian is not uniquely defined. For each of the benchmark models in Tab. I we evaluate the S and T parameters from the full model and from the effective Lagrangian, considering different setups:

- LL-L: *leading-log, loop-induced Wilson coefficients*, where we limit ourselves to the tree-level insertion of loop-induced operators \mathcal{O}_T and $\mathcal{O}_{B,W}$ in the leading-log approximation [22]. Because for testable models the logarithm $\log(\Lambda/m_W)$ cannot be too large, we expect this approximation to not work too well. If we choose the matching scale as $\Lambda = \sqrt{2\lambda_2 v_s^2}$ we find the Wilson coefficients

$$\frac{c_T(\mu)}{\Lambda^2} = -\frac{3\alpha_{ew}s_w^2\lambda_3^2}{32\pi c_w^2\lambda_2\Lambda^2} \log \frac{\Lambda^2}{\mu^2} \quad \frac{c_{B,W}(\mu)}{\Lambda^2} = \frac{\lambda_3^2}{192\pi^2\lambda_2\Lambda^2} \log \frac{\Lambda^2}{\mu^2}. \quad (14)$$

As discussed before, the logarithmic structure of $c_{T,B,W}$ follows from the specific way of breaking custodial symmetry.

- LL-TL: *leading-log, loop-induced Wilson coefficients plus weak-scale loops*, where we add the tree-level induced operator \mathcal{O}_H to the weak-scale loops. These correspond to the SM-like Higgs mediated contributions to the gauge boson polarization, with rescaled Higgs–gauge boson couplings. In addition to the Wilson coefficients given in Eq.(14) we find

$$\frac{c_H}{\Lambda^2} = \frac{\lambda_3^2}{2\lambda_2\Lambda^2}. \quad (15)$$

- LL-TLv: *v-improved leading-log, loop-induced Wilson coefficients plus weak-scale loops*, where we adjust the matching procedure to include v -induced terms [11]. The matching scale is shifted to the mass of the new state, $\Lambda = m_H$. In addition, we express the full model predictions in terms of the mixing angle c_α , so the corresponding Wilson coefficients become

$$\frac{c_H}{\Lambda^2} = \frac{2(1-c_\alpha)}{v^2} \quad \frac{c_T(\mu)}{\Lambda^2} = -\frac{3\alpha_{ew}s_w^2(1-c_\alpha)}{8\pi c_w^2 v^2} \log \frac{m_H^2}{\mu^2} \quad \frac{c_{B,W}(\mu)}{\Lambda^2} = \frac{1-c_\alpha}{48\pi^2 v^2} \log \frac{m_H^2}{\mu^2}. \quad (16)$$

The explicit scale suppression is now replaced by the dependence on the mixing angle with $1-c_\alpha \approx \lambda_3^2 v^2 / (4\lambda_2^2 v_s^2)$, neglecting higher powers of v/v_s . This modification with respect to the default matching is equivalent to resumming part of the higher-dimensional Higgs vev insertions.

- BP-TL: *broken-phase matching, loop-induced Wilson coefficients plus weak-scale loops*, where unlike in the LL-TL scheme we now perform the matching with the full operators in the broken phase. The matching based on Greens functions does not change the Wilson coefficient c_H entering at tree level, but the loop-induced operators which until now are only included with their leading logs. Choosing the default matching scale $\Lambda = \sqrt{2\lambda_2 v_s^2}$ we find

$$\frac{c_T(\mu)}{\Lambda^2} = -\frac{\alpha_{ew}s_w^2\lambda_3^2}{32\pi c_w^2\lambda_2\Lambda^2} \left(-\frac{5}{2} + 3 \log \frac{\Lambda^2}{\mu^2} \right) \quad \frac{c_{B,W}(\mu)}{\Lambda^2} = \frac{\lambda_3^2}{576\pi^2\lambda_2\Lambda^2} \left(-\frac{5}{2} + 3 \log \frac{\Lambda^2}{\mu^2} \right). \quad (17)$$

Compared to the LL-L result in Eq. (14), we obtain a finite term $-5/2$ at order $\mathcal{O}(v^2/\Lambda^2)$ as the genuine contribution from the explicit broken-phase matching.

- BP-TLv: *v-improved broken-phase matching, loop-induced Wilson coefficients plus weak-scale loops*, where we apply the v -improved matching prescription to the BP-TL setup. Both the explicit matching and the v -improvement can now be regarded as strategies to incorporate vev-dependent corrections to the default ideal(ized) effective theory. Combining all improvements we find for the Wilson coefficients

$$\frac{c_T(\mu)}{\Lambda^2} = -\frac{\alpha_{ew}s_w^2(1-c_\alpha)}{8\pi c_w^2 v^2} \left(-\frac{5}{2} + 3 \log \frac{m_H^2}{\mu^2} \right) \quad \frac{c_{B,W}(\mu)}{\Lambda^2} = \frac{1-c_\alpha}{144\pi^2 v^2} \left(-\frac{5}{2} + 3 \log \frac{m_H^2}{\mu^2} \right). \quad (18)$$

This result systematically includes the numerically relevant corrections of order v/Λ to the usual matching scheme.

In Tab.I we introduce a set of benchmark points for the Higgs portal scenario, defining two trajectories in m_H for given $\tan\beta = 10$ and $s_\alpha = 0.1$ or $s_\alpha = 0.3$. The self-couplings are related to the mixing angles through

$$s_\alpha^2 = \frac{m_h^2 - 2\lambda_1 v^2}{m_h^2 - m_H^2}; \quad \tan^2\beta = \frac{v_s^2}{v^2} = \frac{m_h^2 + m_H^2 - 2\lambda_1 v^2}{2\lambda_2 v^2}. \quad (19)$$

	m_H	s_α	$\tan\beta$	$\Lambda = \sqrt{2}\lambda v_s^2$	λ_1	λ_2	λ_3	$c_H v^2/\Lambda^2$	
								LL-TL	BP-TLv
S1	300	0.1	10	298.8	0.13	7.1×10^{-3}	1.2×10^{-2}	6.9×10^{-3}	1.0×10^{-2}
S2	700	0.1	10	696.6	0.16	3.9×10^{-2}	7.5×10^{-2}	9.5×10^{-3}	1.0×10^{-2}
S3	300	0.3	10	288.6	0.18	6.6×10^{-3}	3.4×10^{-2}	6.5×10^{-2}	9.2×10^{-2}
S4	500	0.3	10	668.8	0.46	3.6×10^{-2}	2.2×10^{-1}	9.2×10^{-2}	9.2×10^{-2}

Table I. Benchmark points for the Higgs portal. The Wilson coefficient c_H is given in the default and the v -improved schemes. All mass scales are given in GeV.

In the well-known decoupling limit [23] the two angles are related as $s_\alpha^2 \sim 1/(1 + \tan^2 \beta)$ and for example give $s_\alpha \rightarrow 0$ together with $\beta \rightarrow \pi/2$.

In Table II we evaluate the S and T parameters for the full model and confront the results with the different matching schemes. Default, leading-log matching in the unbroken phase (LL-L) essentially does not reproduce the full model, and even v -improvement (LL-TLv) still leads to a poor agreement with the full prediction. The most accurate BP-TLv setup agrees with the full model typically within a few per-cent. However, we also find sizable discrepancies of up to $\mathcal{O}(30)\%$ for the points S1 and S3, where the relatively low heavy singlet mass ruins the scale hierarchy.

In Fig. 2 we show the decoupling of the oblique parameters for the Higgs portal model and its different dimension-6 approximations. From Eq.(13) we know that both parameters will approach zero in the decoupling limit with a quadratic power suppression, softened by a logarithm $\log(m_H/m_h)$. The leading power suppression arises through the mixing angle α . To reflect this dependence we keep $\lambda_{1,2}$ constant and vary the heavy Higgs mass m_H . Our starting configuration is the benchmark point S4 with $s_\alpha = 0.3$, $\tan\beta = 10$, and $m_H = 300$ GeV. We then decouple the heavy scalar by increasing the physical mass eigenvalue m_H . The lower sub-panels in Fig. 2 correlate the variation of the two mixing angles, which obey $s_\alpha^2 = 1/(a + b \tan^2 \beta)$, with a, b being functions of m_h and $\lambda_{1,2}$. In this situation, the very heavy extra scalar is almost entirely singlet-like, and acquires its large mass through the intrinsic singlet scale $|\mu_s^2| \sim \lambda_2 v_s^2$.

For the S parameter we first observe that not all of the effective Lagrangian approximations give the correct decoupling pattern. Skipping the naive LL-L for now, we see that the leading-log approximation together with the weak-scale loops LL-TL as well as its v -improved counterpart LL-TLv significantly disagree with the full model towards large values of m_H . The situation only improves once we employ a broken-phase matching in our BP-TL scheme, further enhanced significantly in its v -improved version BP-TLv. This tells us that contributions beyond the plain dimension-6 truncation lead to more accurate results only if the complete $\mathcal{O}(v)$ dependence is included. The fact that the simple LL-L approach agrees very well with the full model has to be considered accidental, and we will look at it again below.

Next, we notice that the effective Lagrangians describe the T parameter significantly worse, in particular for small values of the heavy Higgs mass m_H . The reason is its enhanced sensitivity to the relative splittings between m_W , m_Z , and m_h , whereas S really only depends on m_Z . Among the different approximations we still see that only BP-TLv really describes the decoupling accurately, in complete analogy to the S parameter. Unlike for the S parameter, the naive leading-log approximation LL-L exhibits a poor performance, as expected.

The distinguishing feature of the oblique parameters in this model is their delayed decoupling because of the additional logarithm. To study this logarithmic behavior we show the three different definitions of the dimension-6 predictions compared to the full model for fixed s_α in Fig. 3. In the upper panels we show the S parameter for the

		full model	LL-L	LL-TL	LL-TLv	BP-TL	BP-TLv
S	S1	6.22×10^{-4}	4.79×10^{-4}	6.26×10^{-4}	9.15×10^{-4}	4.74×10^{-4}	6.94×10^{-4}
	S2	1.13×10^{-3}	1.08×10^{-3}	1.29×10^{-3}	1.37×10^{-3}	1.08×10^{-3}	1.14×10^{-3}
	S3	5.60×10^{-3}	4.43×10^{-3}	5.83×10^{-3}	8.41×10^{-3}	4.38×10^{-3}	6.38×10^{-3}
	S4	1.01×10^{-2}	1.04×10^{-2}	1.23×10^{-2}	1.26×10^{-2}	1.03×10^{-2}	1.05×10^{-2}
T	S1	-8.30×10^{-4}	-1.39×10^{-3}	-8.07×10^{-4}	-1.18×10^{-3}	-3.67×10^{-4}	-5.41×10^{-4}
	S2	-1.93×10^{-3}	-3.14×10^{-3}	-2.34×10^{-3}	-2.49×10^{-3}	-1.74×10^{-3}	-1.85×10^{-3}
	S3	-7.47×10^{-3}	-1.28×10^{-2}	-7.32×10^{-3}	-1.09×10^{-2}	-3.14×10^{-3}	-4.97×10^{-3}
	S4	-1.74×10^{-2}	-3.00×10^{-2}	-2.22×10^{-2}	-2.29×10^{-2}	-1.63×10^{-2}	-1.70×10^{-2}

Table II. Predictions for S and T in the singlet extension for the full model and the different effective Lagrangian setups. The benchmark points are defined in Tab. I.

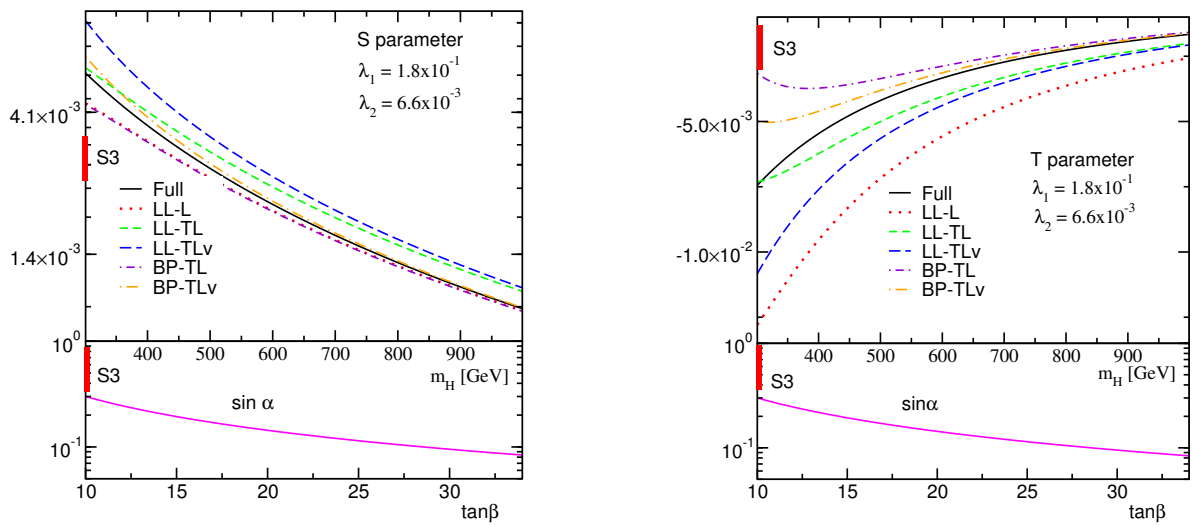


Figure 2. Dependence of S (left) and T (right) on the heavy scalar mass $m_H \approx \Lambda$ towards decoupling. We fix the self-couplings $\lambda_{1,2}$ and compute the mixing angles α and β following Eq.(19) from the varying heavy Higgs mass. The small panels give s_α as a function with $\tan \beta = v_s/v$. The red bar indicates the S4 benchmark point from Tab. I.

two different mixing angles. Following Eq.(12) a larger mixing angle corresponds to a weaker scale hierarchy v/v_s . The benchmark points of Tab. I correspond to the minimum and maximum m_H values.

Again skipping the LL-L setup for the S parameter for now, we start with the standard leading-log LL-TL scenario. While for small m_H this matching scheme seems to agree very well with the full model, at larger m_H we see that this agreement is accidental: increasing the hierarchy of scales and reducing the size of the perturbative parameter (in and beyond the logarithm) makes things significantly worse. This is a clear indication that the leading-log approximation of the Wilson coefficients fails. v -Improving the matching procedure for these leading-log terms in the LL-TLv scheme actually worsens the agreement between the full model and the dimension-6 approximation. For both mixing angles it overshoots the full model description by around 50% for low m_H and 20% for high m_H . As mentioned above, this suggests that in spite of a coincidentally good agreement of the LL-L scheme with the full model the leading-log approximation to the S parameter fails systematically. The behavior of the LL-L curve for $s_\alpha = 0.3$ confirms this picture, because it crosses the full model curve rather than approximating it towards larger m_H .

Extending the full LL-TL scheme to include some v -dependent terms through broken phase matching has a sizeable effect on the effective Lagrangian prediction, as was noted also in Ref. [24]. However, it again does not lead to a significant improvement of the m_H dependence, either. Only the full set of operators computed without the leading-log approximation and including v -induced effects through v -induced matching in the broken phase leads to an agreement of the full model with the effective Lagrangian at 10 ... 15% for low m_H and at 2 ... 4% for large m_H . A crucial consistency check is the appropriate log-modulated decoupling behavior towards large m_H values, which we only observe for the BP-TLv approach.

Moving on to the T parameter we observe a similar behavior. First, unlike in Fig. 2 we do not observe any curves turning over. Instead, we see that this feature is driven by a very poor description of the logarithmic structure in many of the effective Lagrangian approaches. As expected, the LL-L approach now fails badly, adding the weak loops does not improve the too steep dependence on m_H , and v -improvement alone does not help either. Instead, only the properly matched and v -improved BP-TLv scheme leads to an acceptable description of the delayed decoupling of the heavy scalar.

As for the two different ways to improve the matching, we see that v -improvement by itself does not improve the agreement between the dimension-6 approximation and the full model. This illustrates the presence of different orders in the perturbative and the effective Lagrangian expansions: v -improvement resums a subset of $d > 6$ contributions in $(v/\Lambda)^{d-2}$. When computing quantum corrections, this approach is only meaningful if we first ensure that no equally relevant higher-order terms in the perturbative expansion are neglected. Applying v -improvement combined with full broken-phase matching indeed reconciles the dimension-6 results with the full model.

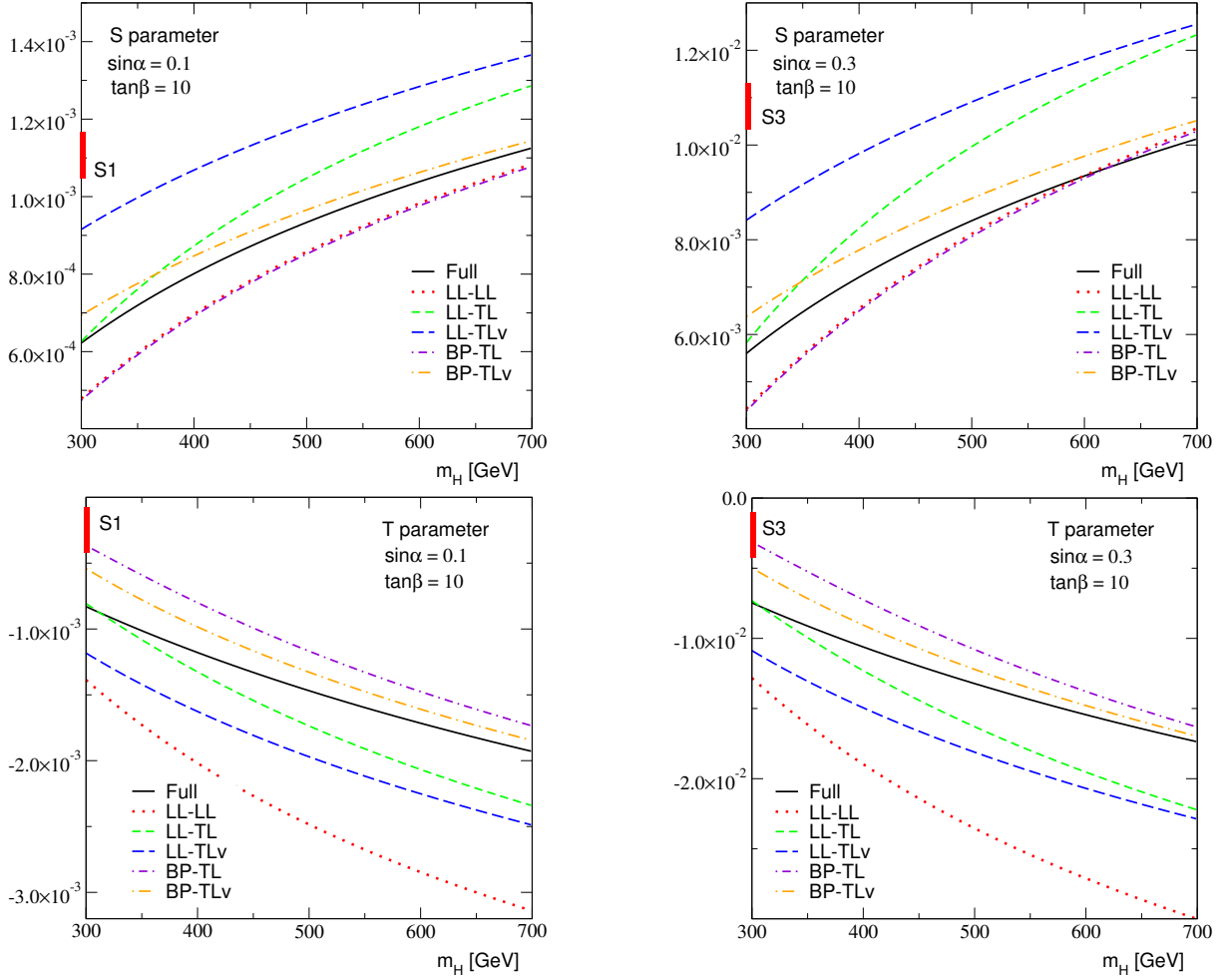


Figure 3. Dependence of the S (upper panels) and T (lower panels) parameters on the heavy scalar mass $m_H \approx \Lambda$ for two choices of mixing angles. Because the mixing angle is kept constant in each panel we only see the logarithmic modulation of the decoupling, shown for example in Eq.(13). The red bar indicates the benchmark points S1 (S4) from Tab. I.

C. Scalar top partners

New colored scalar particles are, strictly speaking, not an extension of the SM Higgs sector, but they can lead to interesting modifications of the LHC observables. We consider a scalar top-partner sector mimicking the stop and sbottom sector of the MSSM. Its Lagrangian has the form[†]

$$\begin{aligned} \mathcal{L} \supset & (D_\mu \tilde{Q})^\dagger (D^\mu \tilde{Q}) + (D_\mu \tilde{t}_R)^* (D^\mu \tilde{t}_R) - \tilde{Q}^\dagger M_{\tilde{Q}_L}^2 \tilde{Q} - M_{\tilde{T}_R}^2 \tilde{t}_R^* \tilde{t}_R \\ & - \kappa_{LL} (\phi \cdot \tilde{Q})^\dagger (\phi \cdot \tilde{Q}) - \kappa_{RR} (\tilde{t}_R^* \tilde{t}_R) (\phi^\dagger \phi) - [\kappa_{LR} \tilde{t}_R^* (\phi \cdot \tilde{Q}) + \text{h.c.}]. \end{aligned} \quad (20)$$

Here, \tilde{Q} and \tilde{t}_R are the additional isospin doublet and singlet in the fundamental representation of $SU(3)_C$. The singlet state \tilde{b}_R is assumed to be heavier and integrated out. This leaves us with three physical degrees of freedom, the scalars \tilde{t}_1 , \tilde{t}_2 and $\tilde{b} = \tilde{b}_L$. The reminiscent underlying R-parity precludes any linear coupling involving the heavy fields. Thus there are no contributions to the oblique parameters proportional to a tree-induced Wilson coefficient

[†] Unlike for example in Ref.[11] we now define κ_{LR} with a mass dimension, because its potential suppression scale is not uniquely defined once we include different loop-level matching schemes.

inside weak-scale loops. The non-Higgs scalar mass matrix has the form

$$\begin{pmatrix} M_{\tilde{Q}_L}^2 + \kappa_{LL} \frac{v^2}{2} & \kappa_{LR} \frac{v}{\sqrt{2}} \\ \kappa_{LR} \frac{v}{\sqrt{2}} & M_{\tilde{T}_R}^2 + \kappa_{RR} \frac{v^2}{2} \end{pmatrix}. \quad (21)$$

After diagonalization we can write the physical top partner masses such that they reflect the scale hierarchies of the effective Lagrangian,

$$\begin{aligned} m_{\tilde{t}_1}^2 &= M_{\tilde{Q}_L}^2 c_{\tilde{t}}^2 + M_{\tilde{T}_R}^2 s_{\tilde{t}}^2 + \frac{v^2}{2} \left(\kappa_{LL} c_{\tilde{t}}^2 + \kappa_{RR} s_{\tilde{t}}^2 + \frac{\sqrt{2}\kappa_{LR}}{v} s_{2\tilde{t}} \right) \approx M^2 + \frac{v^2}{2} \left(\kappa_{LL} c_{\tilde{t}}^2 + \kappa_{RR} s_{\tilde{t}}^2 + \frac{\sqrt{2}\kappa_{LR}}{v} s_{2\tilde{t}} \right) \\ m_{\tilde{t}_2}^2 &= M_{\tilde{Q}_L}^2 s_{\tilde{t}}^2 + M_{\tilde{T}_R}^2 c_{\tilde{t}}^2 + \frac{v^2}{2} \left(\kappa_{LL} s_{\tilde{t}}^2 + \kappa_{RR} c_{\tilde{t}}^2 - \frac{\sqrt{2}\kappa_{LR}}{v} s_{2\tilde{t}} \right) \approx M^2 + \frac{v^2}{2} \left(\kappa_{LL} s_{\tilde{t}}^2 + \kappa_{RR} c_{\tilde{t}}^2 - \frac{\sqrt{2}\kappa_{LR}}{v} s_{2\tilde{t}} \right) \\ m_{\tilde{b}}^2 &= M_{\tilde{Q}_L}^2 \approx M^2, \end{aligned} \quad (22)$$

where $s_{\tilde{t}} = \sin \theta_{\tilde{t}}$ and $c_{\tilde{t}} = \cos \theta_{\tilde{t}}$, etc. The stop mixing angle itself also depends on M and the κ_j , but we keep it in Eq.(22) in the interest of a compact formula. Also shown are the simplified results when assuming a single heavy mass scale $M \equiv M_{\tilde{Q}_L} = M_{\tilde{T}_R}$. Independently of this approximation, the physical mass eigenstates exhibit a mass splitting of $\mathcal{O}(v^2/M^2)$ after electroweak symmetry breaking. A detailed description of the model can be found in the Appendix of Ref. [11].

Assuming, in addition, small mixing $s_{\tilde{t}} \ll 1$ we can approximate the mass spectrum as

$$m_{\tilde{t}_1}^2 \approx M^2 + \frac{\kappa_{LL} v^2}{2} \quad m_{\tilde{t}_2}^2 \approx M^2 + \frac{\kappa_{RR} v^2}{2} \quad m_{\tilde{b}}^2 = M^2. \quad (23)$$

In that limit the oblique parameters have a particularly simple analytical form,

$$\alpha_{\text{em}} T \approx \frac{\kappa_{LL}^2 v^2}{64\pi s_w^2 m_W^2} \frac{v^2}{M^2} \approx \frac{(m_{\tilde{t}_1}^2 - m_{\tilde{b}}^2)^2}{16\pi s_w^2 m_W^2 m_b^2} \quad \text{and} \quad S \approx -\frac{m_{\tilde{t}_1}^2 - m_{\tilde{t}_2}^2}{12\pi m_b^2}. \quad (24)$$

Just as for the portal model, in the following we numerically test different approaches to the dimension-6 operator matching for a set of benchmark points given in Tab. III. Unlike for the Higgs portal model, there is no logarithmic term $\log \Lambda/\mu$ in the scalar top partner model at one-loop level. The relevant matching schemes are:

- SP1: *default matching*, in which the full model is matched to the dimension-6 effective Lagrangian in the unbroken phase, and assuming degenerate heavy masses $M \equiv M_{\tilde{Q}_L} = M_{\tilde{T}_R}$ [15]. As an example, we show the Wilson coefficient contributing to the T parameter,

$$\frac{c_T}{\Lambda^2} = \frac{1}{4(4\pi)^2 M^2} \left[\kappa_{LL}^2 - \frac{\kappa_{LR}^2 \kappa_{LL}}{2 M^2} + \frac{\kappa_{LR}^4}{10 M^4} \right]. \quad (25)$$

The approximate form for T shown in Eq.(24) arises already from the first term or in the limit $\kappa_{LR} \rightarrow 0$.

- SP2: *non-degenerate masses*, where the heavy fields are integrated out following Ref. [13, 25], allowing for two different mass scales $M_{\tilde{Q}_L} \neq M_{\tilde{T}_R}$. For c_T we find

$$\begin{aligned} \frac{c_T}{\Lambda^2} &= \frac{\kappa_{LL}^2}{4(4\pi)^2 M_{\tilde{Q}_L}^2} - \frac{\kappa_{LR}^2 \kappa_{LL}}{2(4\pi)^2} \left[\frac{-5 M_{\tilde{Q}_L}^2 M_{\tilde{T}_R}^2 + M_{\tilde{Q}_L}^4 - 2 M_{\tilde{T}_R}^4}{2 M_{\tilde{Q}_L}^2 (M_{\tilde{Q}_L}^2 - M_{\tilde{T}_R}^2)^3} + \frac{3 M_{\tilde{T}_R}^4}{(M_{\tilde{Q}_L}^2 - M_{\tilde{T}_R}^2)^4} \log \frac{M_{\tilde{Q}_L}^2}{M_{\tilde{T}_R}^2} \right] \\ &+ \frac{\kappa_{LR}^4}{2(4\pi)^2} \left[\frac{10 M_{\tilde{Q}_L}^2 M_{\tilde{T}_R}^2 + M_{\tilde{Q}_L}^4 + M_{\tilde{T}_R}^4}{2 M_{\tilde{Q}_L}^2 (M_{\tilde{Q}_L}^2 - M_{\tilde{T}_R}^2)^4} + \frac{3 M_{\tilde{T}_R}^2 (M_{\tilde{Q}_L}^2 + M_{\tilde{T}_R}^2)}{(M_{\tilde{T}_R}^2 - M_{\tilde{Q}_L}^2)^5} \log \frac{M_{\tilde{Q}_L}^2}{M_{\tilde{T}_R}^2} \right]. \end{aligned} \quad (26)$$

This form reduces to Eq.(25) in the limit of one mass scale only.

- *SPv: v-improved matching*, where the two heavy scales $M_{\tilde{Q}_L}$ and $M_{\tilde{T}_R}$ are traded for $m_{\tilde{t}_1} \approx m_{\tilde{b}}$ and $m_{\tilde{t}_2}$, respectively. We then find

$$\begin{aligned} \frac{c_T}{\Lambda^2} = & \frac{\kappa_{LL}^2}{4(4\pi)^2 m_{\tilde{t}_1}^2} - \frac{\kappa_{LR}^2 \kappa_{LL}}{2(4\pi)^2} \left[\frac{-5m_{\tilde{t}_1}^2 m_{\tilde{t}_2}^2 + m_{\tilde{t}_1}^4 - 2m_{\tilde{t}_2}^4}{2m_{\tilde{t}_1}^2 (m_{\tilde{t}_1}^2 - m_{\tilde{t}_2}^2)^3} + \frac{3m_{\tilde{t}_2}^4}{(m_{\tilde{t}_1}^2 - m_{\tilde{t}_2}^2)^4} \log \frac{m_{\tilde{t}_1}^2}{m_{\tilde{t}_2}^2} \right] \\ & + \frac{\kappa_{LR}^4}{2(4\pi)^2} \left[\frac{10m_{\tilde{t}_1}^2 m_{\tilde{t}_2}^2 + m_{\tilde{t}_1}^4 + m_{\tilde{t}_2}^4}{2m_{\tilde{t}_1}^2 (m_{\tilde{t}_1}^2 - m_{\tilde{t}_2}^2)^4} + \frac{3m_{\tilde{t}_2}^2 (m_{\tilde{t}_1}^2 + m_{\tilde{t}_2}^2)}{(m_{\tilde{t}_2}^2 - m_{\tilde{t}_1}^2)^5} \log \frac{m_{\tilde{t}_1}^2}{m_{\tilde{t}_2}^2} \right]. \end{aligned} \quad (27)$$

which has same functional for as in Eq.(26). In this expression the two left-handed masses $m_{\tilde{t}_1}$ and $m_{\tilde{b}}$ can be used interchangeably.

- *BP1: broken-phase matching*, in which case the Wilson coefficients are derived through explicit matching in the broken phase, assuming a single degenerate heavy scale M . We here obtain

$$\begin{aligned} \frac{c_T}{\Lambda^2} = & \frac{1}{640(4\pi)^2 M^2} \left\{ 5(19\kappa_{LL}^2 + 10\kappa_{LL}\kappa_{RR} + 3\kappa_{RR}^2) - 15(3\kappa_{LL} + \kappa_{RR}) \frac{\kappa_{LR}^2}{M^2} + 8 \frac{\kappa_{LR}^4}{M^4} \right. \\ & + \left[20(\kappa_{LL} - \kappa_{RR})(3\kappa_{LL} + \kappa_{RR}) + 5(\kappa_{LL} + \kappa_{RR}) \frac{\kappa_{LR}^2}{M^2} - 9 \frac{\kappa_{LR}^4}{M^4} \right] c_{4\tilde{t}} \\ & \left. + 5 \left[(\kappa_{LL} - \kappa_{RR})^2 + (5\kappa_{LL} - \kappa_{RR}) \frac{\kappa_{LR}^2}{M^2} \right] c_{8\tilde{t}} + \frac{\kappa_{LR}^4}{M^4} c_{12\tilde{t}} \right\}. \end{aligned} \quad (28)$$

As in the expression for the masses in Eq.(22) the appearance of the mixing angles leads to an additional implicit dependence of on mass matrix parameter M and κ_j , which we keep in the interest of a compact formula. However, this additional dependence obscures the link to the simple form of c_T in Eq.(25). The new terms appearing through broken-phase matching, as compared to Eq.(25) are proportional to $s_{\tilde{t}}$ and hence suppressed for weakly-coupled scenarios. This is different from the Higgs portal case, where broken-phase matching captures finite terms without an extra suppression at small mixing, Eq. (17). This difference can again be explained by the fact that scalar partner effects occur though loops, whereas for the Higgs portal both tree-level and loop-induced operators co-exist.

- *BPv: v-improved broken-phase matching*, where two separate heavy scales $m_{\tilde{t}_1}$ and $m_{\tilde{t}_2}$ are included. For c_T , we compute the 1PI two-point Greens function combination $\Pi_{WW}(0) - c_w^2 \Pi_{ZZ}(0)$ in the full model, expand in powers of $v/M_{\tilde{Q}_L}$ and $v/M_{\tilde{T}_R}$ separately, and match to the dimension-6 effective Lagrangian result. Then we replace $M_{\tilde{Q}_L}$ and $M_{\tilde{T}_R}$ by $m_{\tilde{t}_1}$ and $m_{\tilde{t}_2}$ and introduce $\tilde{\kappa}_{LL} = c_{\tilde{t}}^2 \kappa_{LL} + s_{\tilde{t}}^2 \kappa_{RR}$ and $\tilde{\kappa}_{RR} = s_{\tilde{t}}^2 \kappa_{LL} + c_{\tilde{t}}^2 \kappa_{RR}$. The result is lengthy, but we can illustrate its main features by retaining the leading dependence on the splitting $(m_{\tilde{t}_2}^2 - m_{\tilde{t}_1}^2)/m_{\tilde{t}_2}^2$,

$$\begin{aligned} \frac{c_T}{\Lambda^2} \supset & \frac{(m_{\tilde{t}_2}^2 - m_{\tilde{t}_1}^2)}{2560(4\pi)^2 m_{\tilde{t}_2}^4 v^4} \left\{ 56\kappa_{LR}^4 - \kappa_{LR}^2 m_{\tilde{t}_2}^2 [240\tilde{\kappa}_{LL} + 48\tilde{\kappa}_{RR}] + m_{\tilde{t}_2}^4 [295\tilde{\kappa}_{LL}^2 + 90\tilde{\kappa}_{LL}\tilde{\kappa}_{RR} + 15\tilde{\kappa}_{RR}^2] \right. \\ & - 4 \left[12\kappa_{LR}^4 - \kappa_{LR}^2 (5\tilde{\kappa}_{LL} + 11\tilde{\kappa}_{RR}) m_{\tilde{t}_2}^2 + 5(-15\tilde{\kappa}_{LL}^2 + 2\tilde{\kappa}_{LL}\tilde{\kappa}_{RR} + \tilde{\kappa}_{RR}^2) m_{\tilde{t}_2}^4 \right] c_{4\tilde{t}} \\ & + \left[-24\kappa_{LR}^4 + 16\kappa_{LR}^2 (13\tilde{\kappa}_{LL} + \tilde{\kappa}_{RR}) m_{\tilde{t}_2}^2 + 5(9\tilde{\kappa}_{LL}^2 - 10\tilde{\kappa}_{LL}\tilde{\kappa}_{RR} + \tilde{\kappa}_{RR}^2) m_{\tilde{t}_2}^4 \right] c_{8\tilde{t}} \\ & \left. + \kappa_{LR}^2 \left[16\kappa_{LR}^2 + 12(\tilde{\kappa}_{LL} - \tilde{\kappa}_{RR}) m_{\tilde{t}_2}^2 \right] c_{12\tilde{t}} \right\}, \end{aligned} \quad (29)$$

- *BPv'*: The definition of *BPv* above is based on the assumption that $s_{\tilde{t}}$ is small. If that is not the case, one arrives at a more accurate result by performing the expansion of the full model directly in terms of $v/m_{\tilde{t}_1}$ and $v/m_{\tilde{t}_2}$, while keeping the power counting $s_{\tilde{t}} \sim \mathcal{O}(v/M)$ and $m_{\tilde{b}} - m_{\tilde{t}_1} \sim \mathcal{O}(v)$. One then finds

$$\begin{aligned} \frac{c_T}{\Lambda^2} = & \frac{1}{16\pi^2 v^4} \left[3s_{\tilde{t}}^4 \left(m_{\tilde{t}_1}^2 + m_{\tilde{t}_2}^2 + \frac{2m_{\tilde{t}_1}^2 m_{\tilde{t}_2}^2}{m_{\tilde{t}_2}^2 - m_{\tilde{t}_1}^2} \log \frac{m_{\tilde{t}_1}^2}{m_{\tilde{t}_2}^2} \right) \right. \\ & \left. + \frac{3s_{\tilde{t}}^2 (m_{\tilde{b}}^2 - m_{\tilde{t}_1}^2)}{m_{\tilde{t}_2}^2 - m_{\tilde{t}_1}^2} \left(3m_{\tilde{t}_2}^2 - m_{\tilde{t}_1}^2 - \frac{2m_{\tilde{t}_2}^2}{m_{\tilde{t}_2}^2 - m_{\tilde{t}_1}^2} \log \frac{m_{\tilde{t}_1}^2}{m_{\tilde{t}_2}^2} \right) + \frac{(m_{\tilde{b}}^2 - m_{\tilde{t}_1}^2)^2}{m_{\tilde{t}_1}^2} \right] \end{aligned} \quad (30)$$

Note that Eq.(30) is consistently of order $\mathcal{O}(v^2/M^2)$ as required by the EFT approach.

	$M_{\tilde{Q}_L}$	$M_{\tilde{T}_R}$	κ_{LL}	κ_{RR}	κ_{LR}	$m_{\tilde{t}_1}$	$m_{\tilde{t}_2}$	$m_{\tilde{b}}$	$\theta_{\tilde{t}}$	$c_T v^2 / \Lambda^2$			
										SP1	SP v	BP v	BP v'
P1	500	500	-0.34	0.00	0.58	490	500	500	-0.01	4.23×10^{-5}	4.41×10^{-5}	4.40×10^{-5}	4.40×10^{-5}
P2	500	500	0.066	2.89	74.5	500	580	500	-0.15	1.35×10^{-6}	5.69×10^{-6}	2.76×10^{-6}	1.38×10^{-6}
P3	490	500	0.1	0.1	0.1	493	503	490	-0.0017	3.71×10^{-6}	3.82×10^{-6}	3.82×10^{-6}	3.82×10^{-6}
P4	450	500	0.1	0.1	0.1	453	503	450	-0.00036	3.71×10^{-6}	4.52×10^{-6}	4.52×10^{-6}	4.52×10^{-6}

Table III. Benchmark points for the scalar partner model, where all masses are given in GeV.

For our numerical analysis, we again define some benchmark points in Tab. III. For P1 we assume a single heavy mass scale M and small mixing angle $\theta_{\tilde{t}}$, leading to mild mass splittings between the physical heavy-quark partners; for P2 we also use a single heavy mass scale M but a larger mixing angle from a stronger coupling to the Higgs sector; P3 and P4 both have non-degenerate top partners driven by non-degenerate heavy mass scales in the unbroken phase, $M_{\tilde{Q}_L} \neq M_{\tilde{T}_R}$. For these two scenarios the mixing angle is tiny.

In Tab. IV we show the S and T parameters for the different matching schemes and each of the benchmark points. In general, the effective Lagrangian succeeds in reproducing the full results when the new physics is weakly coupled and relatively heavy, *e.g.* for P1. Small mass splittings $m_{\tilde{t}_1}^2 - m_{\tilde{t}_2}^2 \ll M_{\tilde{T}_R}^2$ are compatible with the assumption of a single heavy scale in the default matching setup. In this weakly-coupled, small mixing regime the v -improved corrections have a tiny numerical impact. A challenge for the effective Lagrangian is a larger mass splitting. This occurs in the unbroken phase when $M_{\tilde{Q}_L} \neq M_{\tilde{T}_R}$. In this case, illustrated by P3 and P4, v -improvement corrects for these $\mathcal{O}(m_{\tilde{t}_1}^2 - m_{\tilde{t}_2}^2)$ key effects in the oblique parameters (24). On the other hand, the use of v -improvement becomes less straightforward for the case of large mixing, as illustrated by P2. The SP v and BP v schemes, which are based on the assumption that the $\hat{1}$ and $\hat{2}$ are closely aligned with the \tilde{Q} and \tilde{t}_R states, differ drastically from the full model. On the other hand, the BP v' scheme, based on a direct expansion in $1/m_{\tilde{t}_{1,2}}$ reproduces all benchmark scenarios very well. Thus it is important to note that the principle of v -improved matching is not uniquely defined, but its optimal implementation needs to be worked out separately for each specific model.

In Fig. 4 we see that all matching schemes essentially follow the expected decoupling behavior at the few per-cent level. Differences appear from the way the different schemes account for the non-degenerate top partner masses. Enhancing the mass splitting leads to significantly larger deviations from the full model for effective Lagrangian setups where only one single mass scale is assumed.

Furthermore, we observe a remarkable contribution from the vev-dependent contributions of dimension greater than six, included via v -improvement; for our parameter choices they flip the sign of the deviations from the full model. Such a systematic positive (negative) offset can be understood by the comparably weaker suppression of the v -improved Wilson coefficients, which scale as inverse powers of the physical masses $c_i \sim 1/m_{\tilde{t}_i}^2$, one of them being lighter than the intrinsic heavy mass scales. A similar trend is observed for the scalar singlet effective Lagrangian in Fig. 2, although the behavior there is affected by logarithmic modulations and sensitive to the additional v -improved replacement $\lambda_3^2/(2\lambda_2) \rightarrow 2(1 - \cos \alpha)$.

The additional improvement from broken phase matching is barely visible for each of the scenarios. This is due to the fact that in the scalar top model there are no contributions with both heavy particles and SM particles in the loop, in contrast to the Higgs singlet model. For the mixed heavy-light loops, the broken-phase matching leads to important differences due to the non-negligible mass of the SM gauge and Higgs bosons.

As complementary information we show the $M_{\tilde{T}_R}$ -dependence of the Wilson coefficients c_T in Fig. 5. We now compare the different matching schemes to the BP v choice, which includes broken-phase matching, v -improvement,

		full model	SP1	SP2	SP v	BP1	BP v	BP v'
S	P1	0.11×10^{-2}	0.11×10^{-2}	0.11×10^{-2}	0.11×10^{-2}	0.11×10^{-2}	0.11×10^{-2}	0.11×10^{-2}
	P2	-0.15×10^{-3}	-0.13×10^{-3}	-0.13×10^{-3}	-0.34×10^{-3}	-0.58×10^{-3}	-0.60×10^{-3}	-0.15×10^{-3}
	P3	-0.32×10^{-3}	-0.31×10^{-3}	-0.31×10^{-3}	-0.32×10^{-3}	-0.31×10^{-3}	-0.32×10^{-3}	-0.32×10^{-3}
	P4	-0.38×10^{-3}	-0.31×10^{-3}	-0.38×10^{-3}	-0.38×10^{-3}	-0.31×10^{-3}	-0.38×10^{-3}	-0.38×10^{-3}
T	P1	0.55×10^{-2}	0.54×10^{-2}	0.54×10^{-2}	0.56×10^{-2}	0.54×10^{-2}	0.56×10^{-2}	0.56×10^{-2}
	P2	0.18×10^{-3}	0.17×10^{-3}	0.17×10^{-3}	0.78×10^{-3}	0.17×10^{-3}	0.35×10^{-2}	0.18×10^{-3}
	P3	0.49×10^{-3}	0.48×10^{-3}	0.48×10^{-3}	0.49×10^{-3}	0.48×10^{-3}	0.49×10^{-3}	0.49×10^{-3}
	P4	0.58×10^{-3}	0.48×10^{-3}	0.48×10^{-3}	0.58×10^{-3}	0.48×10^{-3}	0.58×10^{-3}	0.58×10^{-3}

Table IV. Predictions for S and T in the scalar partner extension for the full model and the different effective Lagrangian setups. The benchmark points are defined in Tab. III.

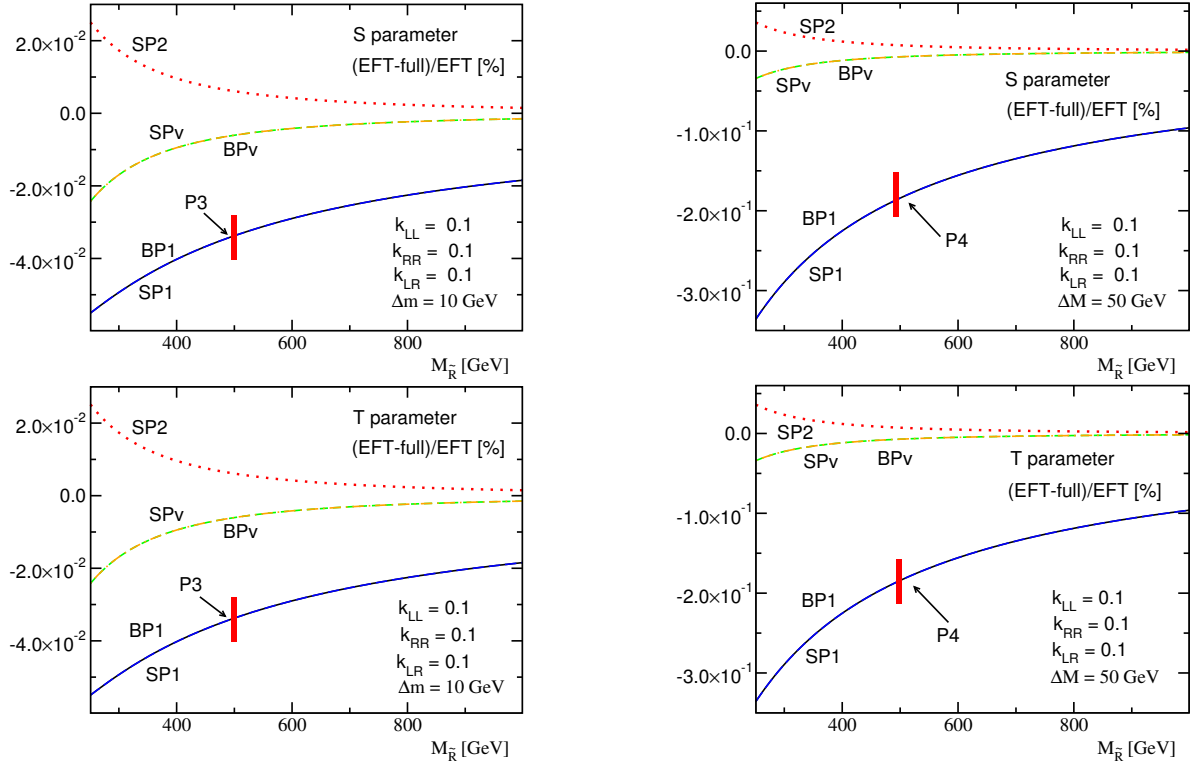


Figure 4. Deviation of S and T from the full model prediction as a function of $M_{\tilde{T}_R}$. We consider two mass splittings $\Delta M \equiv M_{\tilde{T}_R} - M_{\tilde{Q}_L} = 10$ GeV (left) and 50 GeV (right). The red marks indicate the benchmark points P3 and P4 from Tab. III.

and non-degenerate heavy mass scales. The lower panels illustrate the consistent evolution of the top partner mixing angle towards the decoupling limit. Again, for matching prescriptions assuming a single heavy scale we observe deviations rapidly increasing with the scale separation ΔM .

As alluded to above, large mass splittings are the most serious obstacle in constructing an accurate effective description of the heavy scalar partner sector, in particular when they emerge in the broken phase via large couplings κ_i . For Fig. 6 we introduce a mass splitting in the broken phase with $m_{\tilde{t}_1} + \Delta M = m_{\tilde{t}_2} = m_{\tilde{b}} = M$, where M sets a common mass scale of the heavy gauge eigenstates $M_{\tilde{Q}_L} = M_{\tilde{T}_R} = M$, and ΔM is generated primarily through the v -induced κ_{LL} term in Eq.(22). We consider three different values for M and a mixing angle $\theta_{\tilde{t}} = -0.01$. For each value of ΔM we show the relative deviation of the effective Lagrangian prediction from the full model in the left and center panels. The right panel shows the corresponding variation of the couplings κ_j . In general, decoupling leads to decreasing discrepancies between the full model and the effective theory. With increased Higgs couplings, the mass splittings and thus the deviations increase. Interestingly, the observed departures show some systematic behavior, with default matching underestimating and v -improved matching overestimating the full model results. This can be understood as follows: in the limit of small mixing $s_{\tilde{t}}$ and small mass differences ΔM , the results for the T parameter in full model, the default matching (SP1), and the v -improved broken-phase matching (BP v) can be approximated as

$$\begin{aligned}
 \alpha_{\text{em}} T_{\text{full}} &= \frac{(m_{\tilde{t}_2}^2 - m_{\tilde{t}_1}^2)^2}{8\pi s_w^2 m_W^2 (m_{\tilde{t}_1}^2 + m_{\tilde{t}_2}^2)} + \mathcal{O}(s_{\tilde{t}}, (\Delta M)^4) \\
 \alpha_{\text{em}} T_{\text{SP1}} &= \frac{(m_{\tilde{t}_2}^2 - m_{\tilde{t}_1}^2)^2}{16\pi s_w^2 m_W^2 m_{\tilde{t}_2}^2} + \mathcal{O}(s_{\tilde{t}}, (\Delta M)^4) \\
 \alpha_{\text{em}} T_{\text{BP}v} &= \frac{(m_{\tilde{t}_2}^2 - m_{\tilde{t}_1}^2)^2}{16\pi s_w^2 m_W^2 m_{\tilde{t}_1}^2} + \mathcal{O}(s_{\tilde{t}}, (\Delta M)^4).
 \end{aligned} \tag{31}$$

Due to the mass splitting $m_{\tilde{t}_2} - m_{\tilde{t}_1} > 0$, one thus obtains $T_{\text{SP1}} < T_{\text{full}} < T_{\text{BP}v}$ in the scenario in Fig. 6. Similar relations hold for the S parameter.

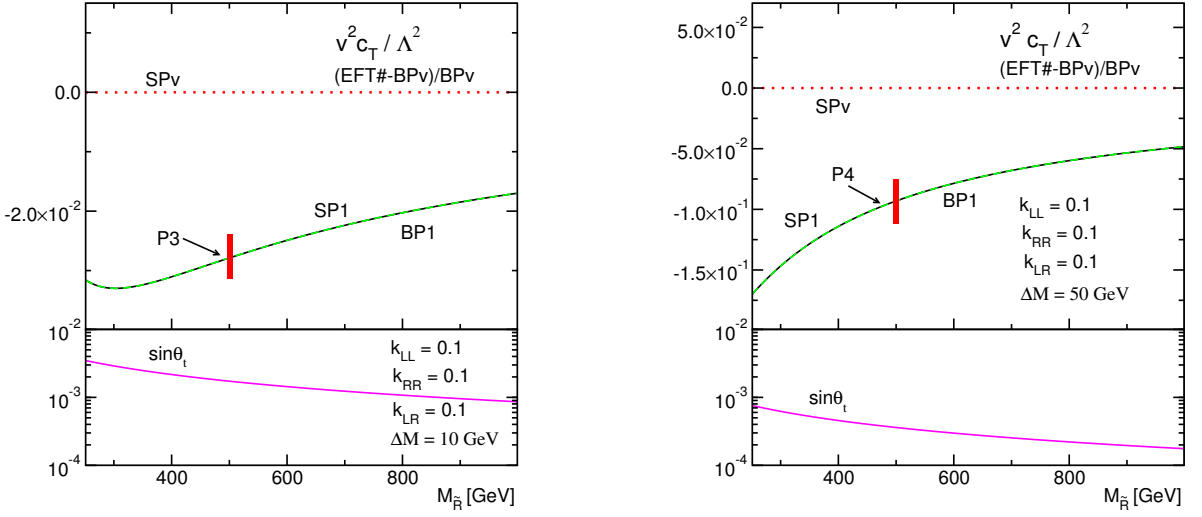


Figure 5. Wilson coefficient c_T as a function of the heavy partner mass $M_{\tilde{T}_R}$. The different curves show the relative deviation between the different setups relative to BPv. We consider two mass splittings $\Delta M \equiv M_{\tilde{T}_R} - M_{\tilde{Q}_L} = 10$ GeV (left) and 50 GeV (right). The red marks indicate the benchmark points P3 and P4 from Tab. III. The decoupling behavior of the stop mixing angle is shown in the lower sub-panels.

Thus both SP1 and BPv deviate from the full model due to v -induced effects, which in this case are not captured by the v -improvement, but are intrinsic to the EFT expansion itself.

III. HIGGS DECAY TO PHOTONS

While LHC observables in general are dominated by tree-level effects from new physics, there are a few select operators where loop-level modifications can make a difference. These include the Wilson coefficients c_γ and c_g , since also in the Standard Model they are generated only at the loop level. This is why in many parametrizations these Wilson coefficients are scaled differently [3]. As part of our analysis of loop effects, we include contributions to the decay $h \rightarrow \gamma\gamma$ of the SM-like Higgs from electrically charged heavy states in the loop. For example, a charged scalar

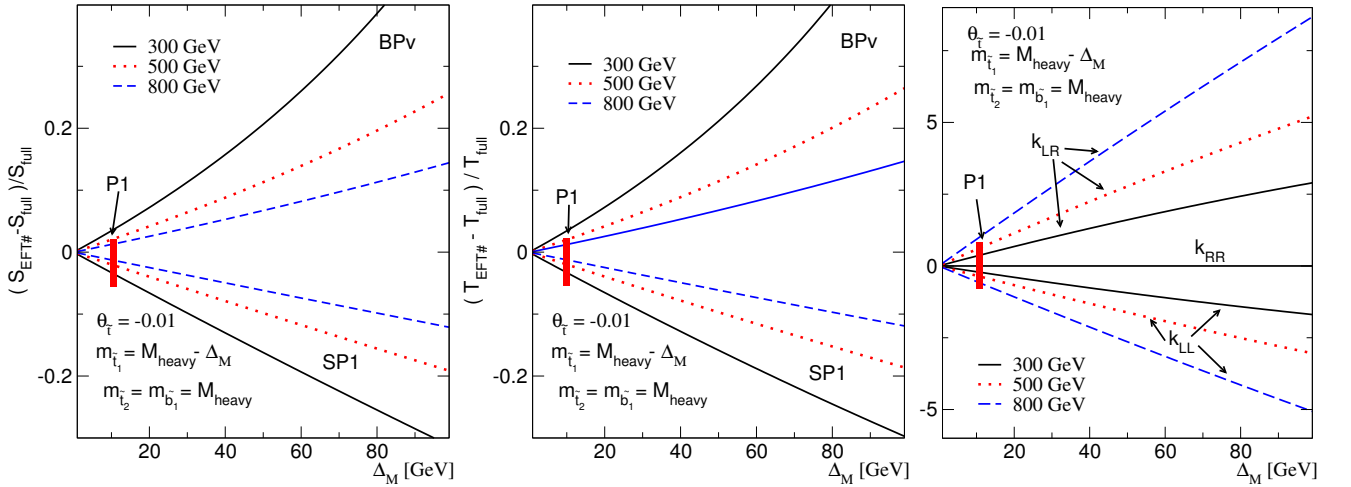


Figure 6. Relative difference $(S_{\text{full}} - S_{\text{EFT}})/S_{\text{full}}$ (left) and $(T_{\text{full}} - T_{\text{EFT}})/T_{\text{full}}$ (center) as a function of the mass splitting between the scalar partners. The mixing angle is fixed to $\theta_t = -0.01$. The right panel shows the couplings to the Higgs sector, with κ_{LR} given in units of GeV. The red bar locates the benchmark point P1 from Tab. III.

can be added to the Standard Model contributions, which stem from heavy fermions and the W -boson,

$$\begin{aligned} \mathcal{L} \supset -\frac{g_{h\gamma\gamma}}{4v} F^{\mu\nu} F_{\mu\nu} H \quad \text{with} \quad g_{h\gamma\gamma} &= g_{h\gamma\gamma}^{\text{SM}} - \frac{\alpha_{\text{em}}}{\pi} C_S Q_S^2 \frac{g_{hSS^*v}}{2m_S^2} A_S(\tau_S) \\ &= -\frac{\alpha_{\text{em}}}{\pi} \left[\sum_{f=\ell,b,\tau} C_f Q_f^2 A_f(\tau_f) + A_W(\tau_W) + C_S Q_S^2 \frac{g_{hSS^*v}}{2m_S^2} A_S(\tau_S) \right]. \end{aligned} \quad (32)$$

Here, $F_{\mu\nu}$ is the abelian photon field strength, and C_f and C_S include potential color factors, distinguishing for example charged Higgs bosons from scalar top partners. The $A_{f,W,S}(\tau)$ are loop functions [26], which for on-shell Higgs decays can be expanded in the ratio $1/\tau_j = m_h^2/(4m_j^2)$,

$$\begin{aligned} A_f(\tau) &= \frac{2}{3} + \frac{7}{45\tau} + \frac{4}{63\tau^2} + \frac{52}{1575\tau^3} + \mathcal{O}\left(\frac{1}{\tau^4}\right), \\ A_W(\tau) &= -\frac{7}{2} - \frac{11}{15\tau} - \frac{38}{105\tau^2} - \frac{116}{525\tau^3} + \mathcal{O}\left(\frac{1}{\tau^4}\right), \\ A_S(\tau) &= \frac{1}{6} + \frac{4}{45\tau} + \frac{2}{35\tau^2} + \frac{64}{1575\tau^3} + \mathcal{O}\left(\frac{1}{\tau^4}\right). \end{aligned} \quad (33)$$

As is well known, the size of the loop-induced contributions increases with the spin of particle in the loop, and vectors contribute with opposite sign from fermions and scalars (assuming a positive coupling to the Higgs boson). Finally, the τ dependence relative to the low-energy limit $\tau \rightarrow \infty$ is different as well,

$$\frac{A_f(\tau)}{A_f(\infty)} \approx 1 + 0.06 \frac{m_h^2}{m_f^2}, \quad \frac{A_W(\tau)}{A_W(\infty)} \approx 1 + 0.05 \frac{m_h^2}{m_W^2}, \quad \frac{A_S(\tau)}{A_S(\infty)} \approx 1 + 0.13 \frac{m_h^2}{m_S^2}, \quad (34)$$

with the largest mass-dependent corrections for a scalar loop. Following this lead we will study two models with additional scalars in this section.

A. Effective Lagrangian

In terms of the effective dimension-6 Lagrangian defined in Eq.(3) the effective Higgs-photon interaction is described by the single operator \mathcal{O}_γ . It is generated within the Standard Model and by possible new physics particles at one loop. The corresponding Wilson coefficient is normalized such that the effective $h\gamma\gamma$ interaction becomes

$$\mathcal{L} \supset -\frac{1}{4v} \left(g_{h\gamma\gamma}^{\text{SM}} - c_\gamma \frac{16\pi \alpha_{\text{em}} v^2}{\Lambda^2} \right) F^{\mu\nu} F_{\mu\nu} H \quad (35)$$

This coupling generates a modified $h \rightarrow \gamma\gamma$ decay width of

$$\Gamma(h \rightarrow \gamma\gamma) = \frac{m_H^3 G_F}{32\pi \sqrt{2}} \left| g_{h\gamma\gamma}^{\text{SM}} - c_\gamma \frac{16\pi \alpha_{\text{em}} v^2}{\Lambda^2} \right|^2. \quad (36)$$

As long as we are mostly interested in on-shell Higgs decays to photons, there is little to learn from the kinematics of the two photons. We therefore describe new physics effects as well as differences between the full model and the dimension-6 approximation in terms of

$$\epsilon_{\gamma\gamma} = \frac{\Gamma_{\gamma\gamma}}{\Gamma_{\gamma\gamma}^{\text{SM}}} - 1 = \frac{\left| g_{h\gamma\gamma}^{\text{SM}} - c_\gamma \frac{16\pi \alpha_{\text{em}} v^2}{\Lambda^2} \right|^2}{\left| g_{h\gamma\gamma}^{\text{SM}} \right|^2} - 1. \quad (37)$$

Notice that for decay processes that are loop-induced in the full model, such as $h \rightarrow \gamma\gamma$ or $h \rightarrow \gamma Z$, there are no additional contributions to $\epsilon_{\gamma\gamma}$. Effects from mass pole residue modifications or shifts in the SM input parameters, dubbed *residue* ϵ_R and *parametric* ϵ_P corrections in Ref.[15], contribute to higher orders in the effective Lagrangian. Similarly, the leading new physics contributions do not modify the decay kinematics, hence there is no effect from the phase space integration. All these aspects, combined with our conservative choice of benchmark points mean

that, unlike for production-side contribution from effective Lagrangians [12] we can linearize the new physics effects in Eq.(37) without ruining the effective Lagrangian approach altogether.

Since in the following we focus on additional scalars we can combine Eq.(32) and Eq.(35) to arrive at the general structure of the matching condition

$$\frac{c_\gamma}{\Lambda^2} = \frac{C_S Q_S^2}{32\pi^2} \frac{g_{hSS}}{v} \frac{A_S(\tau_S)}{m_S^2} \approx \frac{C_S Q_S^2}{192\pi^2} \frac{g_{hSS}}{v} \frac{1}{m_S^2}, \quad (38)$$

where, as usual, we will study the definition of the matching scale Λ and the treatment of terms suppressed by v/Λ for different new physics models.

B. Higgs doublet extension

The Higgs portal model discussed in Sec. IIB is not well suited to study new physics effects in Higgs decays to photons. The reason is that the additional state is not charged and therefore does not contribute to the loop-induced coupling. Therefore, we here instead consider an extended Higgs sector with a second doublet. It is convenient to work in the so-called Higgs basis with the scalar potential [27]

$$\begin{aligned} V(H_1, H_2) = & Y_1 H_1^\dagger H_1 + Y_2 H_2^\dagger H_2 + Y_3 \left(H_1^\dagger H_2 + \text{h.c.} \right) \\ & + \frac{Z_1}{2} \left(H_1^\dagger H_1 \right)^2 + \frac{Z_2}{2} \left(H_2^\dagger H_2 \right)^2 + Z_3 \left(H_1^\dagger H_1 \right) \left(H_2^\dagger H_2 \right) + Z_4 \left(H_1^\dagger H_2 \right) \left(H_2^\dagger H_1 \right) \\ & + \left[\frac{Z_5}{2} \left(H_1^\dagger H_2 \right)^2 + \left(Z_6 H_1^\dagger H_1 + Z_7 H_2^\dagger H_2 \right) H_1^\dagger H_2 + \text{h.c.} \right]. \end{aligned} \quad (39)$$

In this basis only the H_1 doublet develops a vev, $\langle H_1 \rangle = v$, while $\langle H_2 \rangle = 0$. In terms of the mass eigenstates, the Higgs doublets can be expressed as

$$H_1 = \begin{pmatrix} G^+ \\ \frac{v+h+iG^0}{\sqrt{2}} \end{pmatrix}, \quad H_2 = \begin{pmatrix} H^+ \\ \frac{H+iA^0}{\sqrt{2}} \end{pmatrix}, \quad (40)$$

and mapped back onto the generic basis $\{\Phi_k\}$ through the rotation

$$\begin{pmatrix} H_1 \\ H_2 \end{pmatrix} = \begin{pmatrix} c_\beta & s_\beta \\ -s_\beta & c_\beta \end{pmatrix} \begin{pmatrix} \Phi_1 \\ \Phi_2 \end{pmatrix}, \quad (41)$$

where now both of the doublets develop a non-zero vev $\langle \Phi_k \rangle = v_k/\sqrt{2}$, with $v_1 = v s_\beta$, $v_2 = v c_\beta$. In the Higgs basis all quartic couplings are $SO(2)$ -invariant. The corresponding internal symmetries of the model can be thought of as rotations in a Higgs flavor space. The relation

$$s_{\beta-\alpha} c_{\beta-\alpha} = -\frac{Z_6 v^2}{m_H^2 - m_h^2} \quad (42)$$

neatly separates the decoupling limit $m_H \gg v, m_h$ [28] from alignment without decoupling, $Z_6 \rightarrow 0$ [29].

In general, there exist two sources of new physics contributions to the decay rate $h \rightarrow \gamma\gamma$. First, the SM-like Higgs couplings to the W -boson and the heavy fermions are shifted through the rotation of the Higgs mass eigenstates by an angle α and the rotation of the vevs by an angle β . Second, a charged Higgs loop mediates the effective Higgs-photon coupling following Eq.(32). In our analysis we will focus on the alignment setup, removing the shifted SM-like couplings from our analysis of the Higgs-photon coupling. The only remaining effect then is the charged Higgs loop contribution. For the two-Higgs-doublet model the loop contribution from the charged Higgs is mediated by the triple scalar coupling

$$g_{hH^+H^-} = \frac{1}{v} \left(m_h^2 + 2m_{H^\pm}^2 - \frac{2m_{12}^2}{s_\beta c_\beta} \right) = v Z_3 \quad \text{with} \quad m_{H^\pm}^2 = Y_2 + \frac{Z_3 v^2}{2}, \quad (43)$$

up to corrections of $\mathcal{O}(c_{\beta-\alpha}^2)$. The dimension-two coefficient Y_2 generates the heavy doublet mass scale in the gauge-symmetric phase. In the more familiar basis parameters [30] it is given by $Y_2 = m_{11}^2 c_\beta^2 + m_{22}^2 s_\beta^2 + m_{12}^2 s_{2\beta}$. It also gives the default matching scale in the unbroken phase, $\Lambda^2 = Y_2$.

As always, we illustrate different matching schemes, attempting to systematically improve the agreement between full model and dimension-6 Lagrangian:

- SP1: *default matching*, where the full model is matched to the dimension-6 effective Lagrangian in the unbroken phase. Following the general structure of Eq.(38) and assuming the matching scale $\Lambda^2 = Y_2$, we find the relevant Wilson coefficient

$$\frac{c_\gamma}{\Lambda^2} = \frac{Z_3}{192\pi^2} \frac{1}{Y_2}. \quad (44)$$

- BP1*v*: *v-improved broken-phase matching*, where we obtain c_γ from the (derivative of the) 1PI photon Greens function in the full model and the effective Lagrangian setups, expanding both sides of the identity to $\mathcal{O}(v^2/\Lambda^2)$, and identifying the matching scale Λ with the charged Higgs mass

$$\left. \frac{d\Pi_{\gamma\gamma}}{dp^2} \right|_{p^2=0} = \left. \frac{d\Pi_{\gamma\gamma}^{\text{EFT}}}{dp^2} \right|_{p^2=0} = \frac{8s_w^2 m_W^2}{\Lambda^2} c_\gamma \Rightarrow \frac{c_\gamma}{\Lambda^2} = \frac{Z_3}{192\pi^2} \frac{1}{m_{H^\pm}^2}. \quad (45)$$

As above, we compute the deviation in the Higgs-photon coupling $\epsilon_{\gamma\gamma}$, defined in Eq.(37), in the full model and in the different matching setups. Two benchmark points defined in Tab. V represent two complementary regimes: The first point D1 features a weakly coupled scenario, where the physical heavy Higgs masses are driven by the doublet mass Y_2 . The second point D2 is strongly coupled, and a sizable fraction of the heavy Higgs mass is generated by non-decoupling contributions proportional to v . Both scenarios satisfy all theoretical and experimental constraints on the model, in particular the charged Higgs mass limits from direct searches [31] and flavor observables [32]. Additionally, in the alignment limit the lightest CP-even mass eigenstate exactly mimics the properties of the SM Higgs, and therefore is in excellent agreement with the LHC data.

The alignment condition fixes $\alpha = \beta - \pi/2$. In this limit, without any mixing between the two doublets, it makes no difference whether c_γ is obtained via explicit matching or by integrating out the heavy doublet in the unbroken phase with standard functional methods [33].

Since the Higgs couplings to fermions play no role here, we do not need to choose a specific setup for the Yukawa couplings. Also, with no loss of generality, we may assume all heavy Higgs companions to be mass-degenerate.

We show results for the full model and its two different matching schemes in Tab. V. First, for the full model we see that taking into account the squared term $\propto c_\gamma^2$ in Eq.(37) has no measurable effect, because the charged Higgs effects in general hardly reach the per-cent level. Note that if we attempt to define a benchmark point with order-one deviations from the Standard Model, this picture will of course change, and we would have to adapt our approach [12].

For the weakly interacting benchmark point D1, the full model prediction is quite accurately reproduced by the effective Lagrangian in either of the two matching schemes. For the strongly interacting point D2 the charged Higgs contributions are driven by sizable v -mediated couplings. The deviations in $\epsilon_{\gamma\gamma}$ are one order of magnitude larger than in D1, and the squared terms in c_γ gain a little more relevance. The large values of Z_3 , along with the sizeable split between the default matching scale $\sqrt{Y_2}$ and the charged Higgs mass, explain the sizeable difference between the full model and SP1 matching. On the other hand, broken phase matching, BP1*v*, leads to significant improvement over SP1.

C. Scalar top partners

As a second example, we consider the toy model extending the Standard Model by a set of scalar top partners, introduced in Sec. II C. In the spirit of minimal flavor violation, we assume that only the scalar top partners, but not the bottom partner, have sizeable Higgs couplings,

$$g_{h\gamma\gamma} = -\frac{\alpha_{\text{em}}}{\pi} \left[\sum_{f=t,b,\tau} C_f Q_f^2 A_f(\tau_f) + A_W(\tau_W) + \sum_{\tilde{t}} C_{\tilde{t}} Q_{\tilde{t}}^2 \frac{g_{h\tilde{t}\tilde{t}v}}{2m_{\tilde{t}}^2} A_S(\tau_{\tilde{t}}) \right]. \quad (46)$$

	m_H	m_A	m_{H^\pm}	$\tan\beta$	m_{12}^2	$\sqrt{Y_2}$	Z_3	$\epsilon_{\gamma\gamma}$		
								full model	SP1	BP1 <i>v</i>
D1	350	350	350	2	4.9×10^4	338.6	0.27	$6.62(60) \times 10^{-3}$	6.95×10^{-3}	6.50×10^{-3}
D2	350	350	350	1.5	2.8×10^4	231.2	2.36	$5.85(76) \times 10^{-2}$	6.56×10^{-5}	5.75×10^{-2}

Table V. Benchmark points and predictions for $\epsilon_{\gamma\gamma}$, as defined in Eq.(37), in the 2HDM model and its different matching setups. All masses are given in GeV. For the full model, the digit in brackets accounts for the square of the charged Higgs contribution.

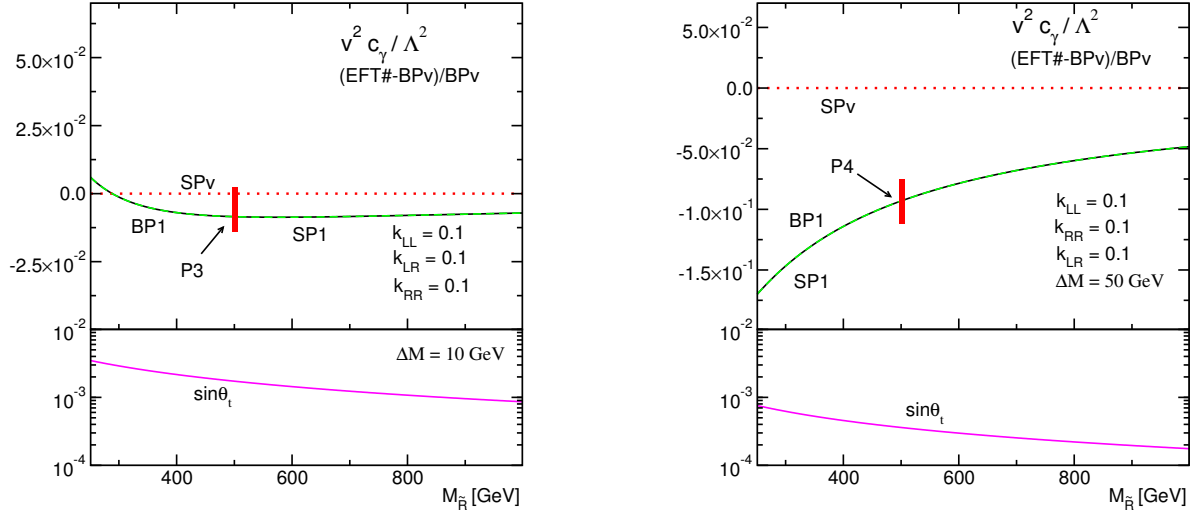


Figure 7. Wilson coefficient c_γ as a function of the heavy partner mass $M_{\tilde{T}_R}$. The different curves show the relative deviation of the different effective Lagrangian predictions relative to the most accurate setup BPv . We consider two mass splittings $\Delta M \equiv M_{\tilde{T}_R} - M_{\tilde{Q}_L} = 10$ GeV (left) and 50 GeV (right). The red marks indicate the benchmark points P3 and P4 from Tab. III. The decoupling behavior of the stop mixing angle is shown in the lower sub-panels.

The heavy top partners couple to the Higgs boson through the off-diagonal entries in their mass matrix,

$$\frac{g_{h\tilde{t}_1\tilde{t}_1}}{v} = \kappa_{LL} c_t^2 + \kappa_{RR} s_t^2 + \frac{\kappa_{LR}}{\sqrt{2}v} s_{2\tilde{t}} \quad \text{and} \quad \frac{g_{h\tilde{t}_2\tilde{t}_2}}{v} = \kappa_{LL} s_t^2 + \kappa_{RR} c_t^2 - \frac{\kappa_{LR}}{\sqrt{2}v} s_{2\tilde{t}}. \quad (47)$$

Along the lines of Eq.(35) we can relate the Higgs–photon couplings in the dimension-6 Lagrangian to the full top partner model as

$$\frac{c_\gamma}{\Lambda^2} = \frac{1}{24\pi^2 v} \left[\frac{g_{h\tilde{t}_1\tilde{t}_1}}{m_{\tilde{t}_1}^2} A_S(\tau_1) + \frac{g_{h\tilde{t}_2\tilde{t}_2}}{m_{\tilde{t}_2}^2} A_S(\tau_2) \right]. \quad (48)$$

To see how accurately the full model prediction for the Higgs-photon coupling $\epsilon_{\gamma\gamma}$ is approximated by effective Lagrangian we consider the same matching setups as in Sec. II C:

- **SP1: *default matching***, in which the full model is matched to the dimension-6 effective Lagrangian in the unbroken phase at $\Lambda = M$. We assume a common heavy spectrum $M_{\tilde{Q}_L} = M_{\tilde{T}_R} \equiv M$ [15],

$$\frac{c_\gamma}{\Lambda^2} = \frac{1}{144\pi^2 M^2} \left[\kappa_{LL} + \kappa_{RR} - \frac{\kappa_{LR}^2}{M^2} \right]. \quad (49)$$

- **SP2: *non-degenerate masses***, where we work again in the unbroken phase, but integrate out non-degenerate heavy fields with $M_{\tilde{Q}_L} \neq M_{\tilde{T}_R}$ separately [13, 25]

$$\frac{c_\gamma}{\Lambda^2} = \frac{1}{144\pi^2} \left[\frac{\kappa_{LL}}{M_{\tilde{Q}_L}^2} + \frac{\kappa_{RR}}{M_{\tilde{T}_R}^2} - \frac{\kappa_{LR}^2}{M_{\tilde{Q}_L}^2 M_{\tilde{T}_R}^2} \right]. \quad (50)$$

- **SPv: *v-improved matching***, which starting from the above result is defined through the replacements $M_{\tilde{Q}_L} \rightarrow m_{\tilde{t}_1}$, $M_{\tilde{T}_R} \rightarrow m_{\tilde{t}_2}$, $\kappa_{LL} \rightarrow \tilde{\kappa}_{LL}$, and $\kappa_{RR} \rightarrow \tilde{\kappa}_{RR}$

$$\frac{c_\gamma}{\Lambda^2} = \frac{1}{144\pi^2} \left[\frac{c_t^2 \tilde{\kappa}_{LL} + s_t^2 \tilde{\kappa}_{RR}}{m_{\tilde{t}_1}^2} + \frac{s_t^2 \tilde{\kappa}_{LL} + c_t^2 \tilde{\kappa}_{RR}}{m_{\tilde{t}_2}^2} - \frac{\kappa_{LR}^2}{m_{\tilde{t}_1}^2 m_{\tilde{t}_2}^2} \right]. \quad (51)$$

- **BP1: *broken-phase matching***, in which case the Wilson coefficients are derived through explicit matching in the broken phase. For a single heavy mass scale M we find

$$\frac{c_\gamma}{\Lambda^2} = \frac{1}{144\pi^2 M^2} \left[\kappa_{LL} + \kappa_{RR} - \frac{\kappa_{LR}^2 s_{2\tilde{t}}^2}{M^2} \right]. \quad (52)$$

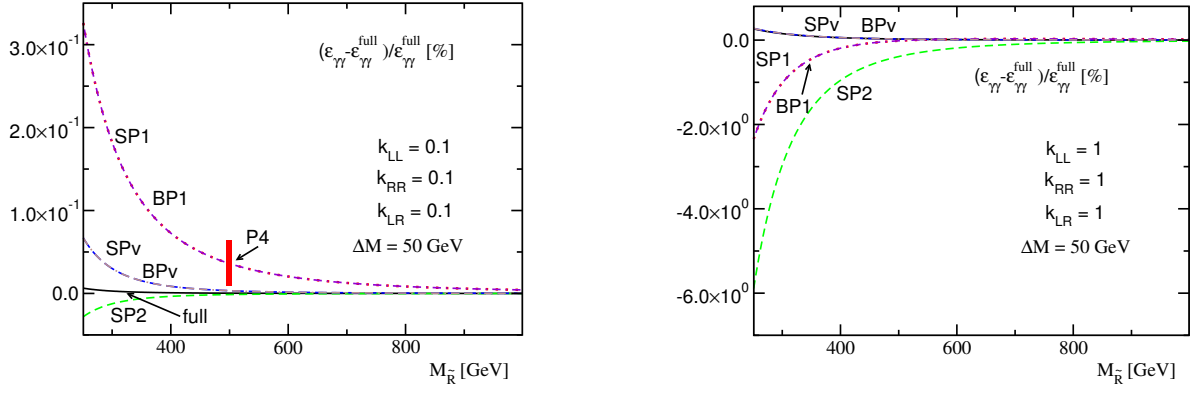


Figure 8. Predictions for $\epsilon_{\gamma\gamma}$, as defined in Eq.(37), as a function of the heavy partner mass $M_{\tilde{T}_R}$. The different curves show the relative deviation between the full model and the effective theory predictions for the different setups. The partner couplings to the Higgs bosons are fixed to weak $\kappa_{LL}, \kappa_{LR}, \kappa_{RR} = 0.1$ (left) and moderate $\kappa_{LL}, \kappa_{LR}, \kappa_{RR} = 1$ values (right). The red mark indicates the benchmark points P4 from Tab. III.

- *BPv*: *v-improved broken-phase matching*, where the different heavy scales in

$$\frac{c_\gamma}{\Lambda^2} = \frac{1}{144 \pi^2} \left[\frac{c_t^2 \kappa_{LL} + s_t^2 \kappa_{RR}}{\tilde{M}_L^2} - \frac{\kappa_{LR}^2 s_{2\tilde{t}}^2}{2\tilde{M}_L^4} + \frac{s_t^2 \kappa_{LL} + c_t^2 \kappa_{RR}}{\tilde{M}_R^2} - \frac{\kappa_{LR}^2 s_{2\tilde{t}}^2}{2\tilde{M}_R^4} \right] \quad (53)$$

are now given by

$$\begin{aligned} \tilde{M}_L^2 &= M_{\tilde{Q}_L}^2 c_t^2 + M_{\tilde{T}_R}^2 s_t^2 \rightarrow m_{\tilde{t}_1}^2 c_t^2 + m_{\tilde{t}_2}^2 s_t^2 \\ \tilde{M}_R^2 &= M_{\tilde{Q}_L}^2 s_t^2 + M_{\tilde{T}_R}^2 c_t^2 \rightarrow m_{\tilde{t}_1}^2 s_t^2 + m_{\tilde{t}_2}^2 c_t^2. \end{aligned} \quad (54)$$

For these different matching setups we compute the modifications to the Higgs-photons coupling $\epsilon_{\gamma\gamma}$, as defined in Eq.(37). We use the same benchmarks as in Sec. II C for the results shown in Tab. VI. The digit in parentheses indicates the change when we add the square of the scalar partner loops. The numerical results are similar to those of the oblique parameters in Sec. II C. The very mild offsets between the simple *v-improved* setup *SPv* and the full broken phase matching scheme *BPv* can be attributed to the $\theta_{\tilde{t}}$ -suppressed contributions in *BPv*. On the other hand, in contrast to the oblique parameters, we find hardly any effect from a non-degenerate spectrum with large mixing. This is related to the diagonal structure of the electromagnetic coupling, which implies that, unlike $c_{W,B,T}$, the one-loop contributions to $\Pi_{\gamma\gamma}$ do not feature a simultaneous exchange of different mass states. Our effective Lagrangian result for c_γ therefore agrees very well with the full model, even for the strongly-coupled scenario P2.

In Fig. 8 we study the decoupling behavior of $\epsilon_{\gamma\gamma}$ as a function of the heavy partner mass $M_{\tilde{T}_R}$. We consider a weakly-coupled scenario with $\kappa_{LL}, \kappa_{LR}, \kappa_{RR} = 0.1$, as in benchmarks P3 and P4, and compare it to the case of $\kappa \sim \mathcal{O}(1)$. We find that the dimension-6 approximation gives an excellent approximation to the full model for $M \gtrsim 400$ GeV for weak couplings and $M \gtrsim 600$ GeV for strong couplings. A comparably more dramatic breakdown of the effective Lagrangian appears for $M \lesssim 400$ GeV in the strongly-coupled case. Large couplings combined with a small scale separation render the default matching approach inadequate, whereas the *v-improved* matching agrees with the full model within less than 1% down to $M \approx 250$ GeV. In contrast to the oblique parameters, no delayed

$\epsilon_{\gamma\gamma}$	full model	SP1	SP2	SPv	BP1	BPv
P1	$0.565(6) \times 10^{-2}$	0.538×10^{-2}	0.538×10^{-2}	0.560×10^{-2}	0.538×10^{-2}	0.560×10^{-2}
P2	$-0.354(1) \times 10^{-1}$	-0.466×10^{-1}	-0.466×10^{-1}	-0.349×10^{-1}	-0.469×10^{-1}	-0.356×10^{-1}
P3	$-0.324(4) \times 10^{-2}$	-0.319×10^{-2}	-0.325×10^{-2}	-0.322×10^{-2}	-0.319×10^{-2}	-0.322×10^{-2}
P4	$-0.355(5) \times 10^{-2}$	-0.319×10^{-2}	-0.356×10^{-2}	-0.352×10^{-2}	-0.319×10^{-2}	-0.352×10^{-2}

Table VI. Predictions for $\epsilon_{\gamma\gamma}$ in the scalar partner model and the different effective Lagrangian setups described in the text. The benchmark points are defined in Tab. III. The digit in brackets accounts for the squared of the scalar partner loops.

decoupling is encountered even for large v -induced mass splitting. As mentioned above, this is due to the fact that the two scalar top partner eigenstates do not mix in the $h\gamma\gamma$ loops.

Some other characteristic trends already encountered in the electroweak precision analysis are again visible in $\epsilon_{\gamma\gamma}$: first, the sign of the deviation flips between the default EFT truncation and the v -improved matching, where the latter reproduces the full model predictions much more accurately. Second, the broken-phase corrections from explicit matching are again negligible since there are no mixed heavy-light loops in the scalar top partner model. For the weakly coupled scenario in the left panel of Fig. 8, we observe unexpectedly good agreement between the SP2 matching, without v -improvement, and the full model. However, this turns out to be simply a numerical coincidence, as can be seen by inspecting the relatively poor performance of SP2 in the scenario in Fig. 8 (right).

IV. SUMMARY

To justify using an effective Lagrangian, for example truncated at dimension six, we need to either show that higher-dimensional contributions are negligible, or that the effective Lagrangian reproduces the features of classes of complete models. In the second case, the appropriate matching procedure can play a key role, in particular if we integrate out particles right around the scale of electroweak symmetry breaking, *i.e.* at a scale where the structure of the Lagrangian changes significantly.

At tree level it is known that taking into account terms of the order v^2/Λ^2 in the definition of the matching scale and in the matching condition can make a sizeable difference [11]. In this paper we have systematically studied possible improvements in the matching procedure at the one-loop level, considering the oblique electroweak parameters S and T , as well as the Higgs decay width to photons. For extended scalar sectors we have confirmed three ways to systematically improve the matching procedure of a dimension-6 Lagrangian with linearly realized electroweak symmetry breaking:

1. v -improving the matching scale and matching condition by expressing them in terms of the (lightest) integrated-out particle mass and mixing angles will improve the agreement with the full model, both at tree level and at loop level;
2. determining the matching condition based on Greens functions in the broken phase and including the appropriate v -suppressed terms can lead to a systematic improvement, if combined with v -improved matching;
3. properly taking into account several new physics scales, if present, to avoid issues with mass splittings induced in the unbroken as well as in the broken phase.

Simple and convenient matching schemes based on leading logarithms [20, 34], in contrast, are not useful for any kind of precision physics. Altogether we have introduced an appropriate matching procedure around the scale of electroweak symmetry breaking, systematically including v -induced effects. We note that it is always possible to find better agreement between full models and the effective with the help of v -improvement, but the appropriate form of the v -suppressed terms depends on the model and the number of scales involved. In particular for the LHC the freedom to optimize the matching procedure will be the key to defining a usable effective Lagrangian approach.

Acknowledgments

First of all we would like to thank Juan González-Fraile for his contributions during an early phase of the project. TP, AF, and DLV would like to thank the MITP, KITPC, and Institut für Theoretische Physik at Karlsruhe for their hospitality while this paper was finished. DLV is funded by the F.R.S.-FNRS *Fonds de la Recherche Scientifique* (Belgium). The work of AF is funded in part by the U.S. National Science Foundation under grant PHY-1519175. DLV also wishes to warmly thank Cen Zhang for more than enlightening discussions.

-
- [1] K. Hagiwara, R. Szalapski and D. Zeppenfeld, Phys. Lett. B **318**, 155 (1993); T. Corbett, O. J. P. Éboli, J. Gonzalez-Fraile and M. C. Gonzalez-Garcia, Phys. Rev. D **86**, 075013 (2012); E. Massó and V. Sanz, Phys. Rev. D **87**, no. 3, 033001 (2013); T. Corbett, O. J. P. Éboli, J. Gonzalez-Fraile and M. C. Gonzalez-Garcia, Phys. Rev. D **87**, 015022 (2013); W. F. Chang, W. P. Pan and F. Xu, Phys. Rev. D **88**, no. 3, 033004 (2013); B. Dumont, S. Fichet and G. von Gersdorff, JHEP **1307**, 065 (2013); C. Y. Chen, S. Dawson and C. Zhang, Phys. Rev. D **89**, no. 1, 015016 (2014); J. Ellis, V. Sanz and T. You, JHEP **1407**, 036 (2014); A. Azatov, C. Grojean, A. Paul and E. Salvioni, Zh. Eksp. Teor. Fiz. **147**, 410 (2015) [J. Exp. Theor. Phys. **120**, 354 (2015)]; C. Englert, Y. Soreq and M. Spannowsky, JHEP **1505**, 145 (2015); J. Ellis, V. Sanz and T. You, JHEP **1503**, 157 (2015); H. Blusca-Mato and A. Falkowski, arXiv:1602.02645 [hep-ph].

- [2] G. F. Giudice, C. Grojean, A. Pomarol and R. Rattazzi, *JHEP* **0706**, 045 (2007); R. Contino, M. Ghezzi, C. Grojean, M. Mühlleitner and M. Spira, *JHEP* **1307**, 035 (2013).
- [3] T. Corbett, O. J. P. Éboli, D. Gonçalves, J. Gonzalez-Fraile, T. Plehn and M. Rauch, *JHEP* **1508**, 156 (2015).
- [4] K. Hagiwara, S. Ishihara, R. Szalapski and D. Zeppenfeld, *Phys. Lett. B* **283**, 353 (1992); T. Corbett, O. J. P. Éboli, J. Gonzalez-Fraile and M. C. Gonzalez-Garcia, *Phys. Rev. Lett.* **111**, 011801 (2013); A. Falkowski, M. Gonzalez-Alonso, A. Greljo and D. Marzocca, *Phys. Rev. Lett.* **116**, no. 1, 011801 (2016); A. Butter, O. J. P. Éboli, J. Gonzalez-Fraile, M. C. Gonzalez-Garcia, T. Plehn and M. Rauch, arXiv:1604.03105 [hep-ph].
- [5] K. Hagiwara, S. Ishihara, R. Szalapski and D. Zeppenfeld, *Phys. Rev. D* **48**, 2182 (1993).
- [6] C. Degrande, J. M. Gerard, C. Grojean, F. Maltoni and G. Servant, *JHEP* **1103**, 125 (2011); D. Y. Shao, C. S. Li, J. Wang, J. Gao, H. Zhang and H. X. Zhu, *Phys. Rev. D* **84**, 054016 (2011); C. Zhang, N. Greiner and S. Willenbrock, *Phys. Rev. D* **86**, 014024 (2012); C. Degrande, J. M. Gerard, C. Grojean, F. Maltoni and G. Servant, *JHEP* **1207**, 036 (2012) Erratum: [*JHEP* **1303**, 032 (2013)]; C. Englert, A. Freitas, M. Spira and P. M. Zerwas, *Phys. Lett. B* **721**, 261 (2013); C. Zhang, *Phys. Rev. D* **90**, 014008 (2014); G. Durieux, F. Maltoni and C. Zhang, *Phys. Rev. D* **91**, 074017 (2015); A. Buckley, C. Englert, J. Ferrando, D. J. Miller, L. Moore, M. Russell and C. D. White, *Phys. Rev. D* **92**, 091501 (2015).
- [7] J. Goodman, M. Ibe, A. Rajaraman, W. Shepherd, T. M. P. Tait and H. B. Yu, *Phys. Lett. B* **695**, 185 (2011); J. Goodman, M. Ibe, A. Rajaraman, W. Shepherd, T. M. P. Tait and H. B. Yu, *Phys. Rev. D* **82**, 116010 (2010); S. Liem, G. Bertone, F. Calore, R. Ruiz de Austri, T. M. P. Tait, R. Trotta and C. Weniger, arXiv:1603.05994 [hep-ph].
- [8] A. Biekötter, A. Knochel, M. Krämer, D. Liu and F. Riva, *Phys. Rev. D* **91**, 055029 (2015).
- [9] C. Arnesen, I. Z. Rothstein and J. Zupan, *Phys. Rev. Lett.* **103**, 151801 (2009); S. Banerjee, S. Mukhopadhyay and B. Mukhopadhyaya, *Phys. Rev. D* **89**, no. 5, 053010 (2014); C. Englert and M. Spannowsky, *Phys. Lett. B* **740**, 8 (2015); M. de Vries, *JHEP* **1503**, 095 (2015); S. Dawson, I. M. Lewis and M. Zeng, *Phys. Rev. D* **91**, 074012 (2015); R. Edezhath, arXiv:1501.00992 [hep-ph]; L. Edelhäuser, A. Knochel and T. Steeger, *JHEP* **1511**, 062 (2015); R. Contino, A. Falkowski, F. Goertz, C. Grojean and F. Riva, arXiv:1604.06444 [hep-ph].
- [10] M. Gorbahn, J. M. No and V. Sanz, *JHEP* **1510**, 036 (2015).
- [11] J. Brehmer, A. Freitas, D. López-Val and T. Plehn, *Phys. Rev. D* **93**, 075014 (2016).
- [12] A. Biekötter, J. Brehmer and T. Plehn, arXiv:1602.05202 [hep-ph].
- [13] A. Drozd, J. Ellis, J. Quevillon and T. You, *JHEP* **1506**, 028 (2015).
- [14] M. K. Gaillard, *Nucl. Phys. B* **268**, 669 (1986); O. Cheyette, *Nucl. Phys. B* **297**, 183 (1988).
- [15] B. Henning, X. Lu and H. Murayama, *JHEP* **1601**, 023 (2016).
- [16] B. Grzadkowski, M. Iskrzynski, M. Misiak and J. Rosiek, *JHEP* **1010**, 085 (2010).
- [17] R. Alonso, E. E. Jenkins and A. V. Manohar, *Phys. Lett. B* **739**, 95 (2014).
- [18] E. Witten, *Nucl. Phys. B* **104**, 445 (1976); M. S. Bilenky and A. Santamaria, *Nucl. Phys. B* **420**, 47 (1994); M. S. Bilenky and A. Santamaria, In *Wendisch-Rietz 1994, Proceedings, Theory of elementary particles 215-224* [hep-ph/9503257]; F. del Aguila, Z. Kunszt and J. Santiago, arXiv:1602.00126 [hep-ph].
- [19] T. Hahn, *Comput. Phys. Commun.* **140**, 418 (2001). T. Hahn and M. Pérez-Victoria, *Comput. Phys. Commun.* **118**, 153 (1999).
- [20] R. Alonso, E. E. Jenkins, A. V. Manohar and M. Trott, *JHEP* **1404**, 159 (2014); J. Elias-Miró, C. Grojean, R. S. Gupta and D. Marzocca, *JHEP* **1405**, 019 (2014); L. Berthier and M. Trott, *JHEP* **1505**, 024 (2015); J. D. Wells and Z. Zhang, *JHEP* **1606**, 122 (2016).
- [21] V. Barger, P. Langacker, M. McCaskey, M. J. Ramsey-Musolf and G. Shaughnessy, *Phys. Rev. D* **77**, 035005 (2008); M. Boggia, R. Gomez-Ambrosio and G. Passarino, arXiv:1603.03660 [hep-ph].
- [22] C. W. Chiang and R. Huo, *JHEP* **1509**, 152 (2015).
- [23] T. Appelquist and J. Carazzone, *Phys. Rev. D* **11**, 2856 (1975); Y. Kazama and Y. P. Yao, *Phys. Rev. D* **25**, 1605 (1982).
- [24] C. Hartmann and M. Trott, *JHEP* **1507**, 151 (2015).
- [25] A. Drozd, J. Ellis, J. Quevillon and T. You, *JHEP* **1603**, 180 (2016).
- [26] A. Djouadi, *Phys. Rept.* **457**, 1 (2008).
- [27] S. Davidson and H. E. Haber, *Phys. Rev. D* **72**, 035004 (2005) Erratum: [*Phys. Rev. D* **72**, 099902 (2005)]; H. E. Haber and D. O'Neil, *Phys. Rev. D* **74**, 015018 (2006); H. E. Haber and D. O'Neil, *Phys. Rev. D* **83**, 055017 (2011); H. E. Haber and O. Stål, *Eur. Phys. J. C* **75**, no. 10, 491 (2015) Erratum: [*Eur. Phys. J. C* **76**, no. 6, 312 (2016)].
- [28] J. F. Gunion and H. E. Haber, *Phys. Rev. D* **67**, 075019 (2003); H. E. Haber, arXiv:1401.0152 [hep-ph].
- [29] M. Carena, I. Low, N. R. Shah and C. E. M. Wagner, *JHEP* **1404**, 015 (2014); A. Delgado, G. Nardini and M. Quirós, *JHEP* **1307**, 054 (2013).
- [30] G. C. Branco, P. M. Ferreira, L. Lavoura, M. N. Rebelo, M. Sher and J. P. Silva, *Phys. Rept.* **516**, 1 (2012).
- [31] J. Abdallah *et al.* [DELPHI Collaboration], *Eur. Phys. J. C* **34**, 399 (2004); G. Abbiendi *et al.* [ALEPH and DELPHI and L3 and OPAL and LEP Collaborations], *Eur. Phys. J. C* **73**, 2463 (2013); CMS Collaboration [CMS Collaboration], CMS-PAS-HIG-14-020; V. Khachatryan *et al.* [CMS Collaboration], *JHEP* **1511**, 018 (2015); B. Coleppa, F. Kling and S. Su, *JHEP* **1412**, 148 (2014).
- [32] B. Aubert *et al.* [BaBar Collaboration], *Phys. Rev. D* **77**, 051103 (2008); S. Su and B. Thomas, *Phys. Rev. D* **79**, 095014 (2009); M. Aoki, S. Kanemura, K. Tsumura and K. Yagyu, *Phys. Rev. D* **80**, 015017 (2009); F. Mahmoudi and T. Hurth, *PoS ICHEP* **2012**, 324 (2013); Y. Amhis *et al.* [Heavy Flavor Averaging Group (HFAG) Collaboration], arXiv:1412.7515 [hep-ex]; M. Misiak *et al.*, *Phys. Rev. Lett.* **114**.
- [33] M. Gorbahn, J. M. No and V. Sanz, *JHEP* **1510**, 036 (2015).
- [34] C. Grojean, E. E. Jenkins, A. V. Manohar and M. Trott, *JHEP* **1304**, 016 (2013); J. Elias-Miró, J. R. Espinosa, E. Masso

and A. Pomarol, JHEP **1311**, 066 (2013); S. Jung, P. Ko, Y. W. Yoon and C. Yu, JHEP **1408**, 120 (2014).